Alma Mater Studiorum – Università di Bologna

Dottorato di Ricerca in Geofisica - XXIV Ciclo

Settore Concorsuale di afferenza: 04/A4
Settore Scientifico disciplinare: GEO/10 Geofisica della Terra Solida

NUMERICAL MODELS OF TRENCH MIGRATION FOR LATERAL HETEROGENEOUS SUBDUCTING PLATES

Presentata da:
Valentina Magni

Coordinatore Dottorato:
Michele Dragoni

Relatore:
Claudio Faccenna

Esame finale anno 2012

ABSTRACT

The aim of this Thesis is to investigate the effect of heterogeneities within the subducting plate on the dynamics of subduction. In particular, I study the motion of the trench for oceanic and continental subduction, first, separately, and, then, together in the same system to understand how they interact. The understanding of these features is fundamental to reconstruct the evolution of complex subduction zones, such as the Central Mediterranean.

For this purpose, I developed 2D and 3D numerical models of oceanic and continental subduction where the rheological, geometrical and compositional properties of the plates are varied. In these models, the trench and the overriding plate move self-consistently as a function of the dynamics of the system (i.e., no external forces are imposed).

The numerical results of models with a purely oceanic slab showed that the presence of lateral age variations within the subducting plate affects the dynamics of subduction. Indeed, the different retreating velocities of the slab along the subduction front lead to the deformation of the overriding plate and, thus, to the formation of a curve trench.

Afterwards, the effect of continental subduction on trench migration is largely investigated. Results from a parametric study showed that despite different rheological properties of the plates, all models of continental subduction with a uniform crust share the same kinematic behaviour: the trench starts to advance once the continent arrives at the subduction zone. Hence, the advancing mode in continental collision scenarios is at least partly driven by an intrinsic feature of the system. Moreover, I found that the presence of a weak lower crust within the continental plate can lead to the occurrence of delamination. In particular, by changing the viscosity of the lower crust and the maximum viscosity of the lithosphere, both delamination and slab detachment can occur. Delamination is favoured by a low viscosity value of the lower crust, because this makes the mechanical decoupling easier between the crust and the lithospheric mantle. These features are observed both in 2D and 3D models, but the numerical results of the 3D models also showed that the rheology of the continental crust has a very strong effect on the dynamics of the whole system, since it influences not only the continental part of plate but also the oceanic sides.

Finally, a better understanding of the dynamics of trench migration in different scenarios allowed me to study the evolution of subduction over the last 40 Myr in the Central Mediterranean with the aim of unravelling how this is related with the main tectonic features recognized in this region. The numerical model was able to reproduce the main tectonic features present in this area (e.g., the formation of a back-arc basin, the fast retreating of the Calabrian slab and the pronounced trench curvature).

TABLE OF CONTENTS

CHAPTER 1

Introduction

1.1 General introduction

Cold, dense subducting lithosphere provides the primary force driving plate tectonic [*Forsyth and Uyeda*, 1975]. The study of the processes that take place inside the Earth is challenging given the lack of direct observations and measurements of physical properties. Tomographic images and analysis of seismic anisotropy provide useful indirect information on mantle structure and circulation. Other indirect data come from geological observations, petrographic and geochemical studies. Since these observations describe only few moments of the ongoing processes, the use of dynamical modelling is necessary to link this information and have a more complete understanding of the evolution of the processes.

The evolution of subducted slabs depends on the balance of driving and resisting forces, how these forces change with depth and time, and the geometry imposed by the larger-scale tectonic environment. Driving forces include ridge-push, the negative buoyancy owing to cold thermal anomalies and elevation of the olivine-to-wadsleyite (α-to-β olivine; spinel-structure) phase transition at a depth of 410 km. Resisting forces include bending of the lithosphere and frictional plate-coupling at shallow depths, viscous shear in the mantle, and positive buoyancy forces owing to the phase transition at a depth of 660 km and, if present, the density anomaly of the continental material. In addition to the local forces, large-scale mantle flow and flow-induced pressure anomalies also affect the sinking rate and geometry of subducting lithosphere. The relative importance of each of the driving and resisting forces depends on the details of the subduction history (e.g., age of the subducting lithosphere, plate boundary dip and mechanical properties, sinking rate, duration of subduction) [*Billen*, 2008].

Geological and seismic observations of convergent margins showed that subduction zones are not steady-state features and that the trench can either move towards the overriding plate (advancing mode) or the subducting plate (retreating mode). The trench motion is influenced by the rheological, geometrical and compositional properties of the slab and its interaction with the upper/lower mantle discontinuity at 660 km of depth. Furthermore, trench migration has important consequences for tectonics such as back-arc spreading, but also for large-scale upper mantle dynamics. Modifications in the oceanic plate areas and trench locations will

affect long-term heat transport and mixing efficiency of mantle convection. Regionally, the motion of trenches is also of importance since the details of mantle flow will be affected [*Becker and Faccenna*, 2009].

In recent decades, many numerical [e.g., *Becker et al.*, 1999; *Christensen*, 1996; *Enns et al.*, 2005; *Garfunkel et al.*, 1986; *Stegman et al.*, 2006; *van Hunen et al.*, 2000; *van Hunen et al.*, 2002; *Zhong and Gurnis*, 1995] and laboratory [e.g., *Bellahsen et al.*, 2005; *Faccenna et al.*, 2007a; *Funiciello et al.*, 2003a; *Funiciello et al.*, 2008; *Griffiths et al.*, 1995; *Heuret et al.*, 2007; *Jacoby*, 1976; *Martinod et al.*, 2005; *Schellart*, 2008; *Shemenda*, 1993] models of subduction have been performed to understand the mechanisms that drive trench migration, giving important insights to a better knowledge of the subduction dynamics. However, key-questions related to the shape of trenches, the amount, direction and velocity of their migration remain open. In particular, the effect of lateral heterogeneities within the subducting plate on trench migration is still poorly understood. The understanding of these features is fundamental to reconstruct the evolution of complex subduction zones, such as the Central Mediterranean. Indeed, the complicated tectonic history of this area is caused by the large rheological, geometrical and compositional variations within a relative small system, which makes difficult a tectonic reconstruction.

In this Thesis, I use the finite element method to model subduction and study some of the key mechanisms that control plate tectonics. I particularly focus on modelling subduction of heterogeneous lithosphere (e.g., different plate age and presence of continental plateau). To do that, I perform both 2D and 3D full dynamical numerical models. One of the main advantages of modelling subduction in a 3D domain is the possibility to include lateral heterogeneities within the plates. The main aims of this work are:

- investigate how geometrical, compositional and rheological parameters of the plates affect trench migration;
- provide an understanding on the role of lateral thickness and density variations within the subducting plate on trench migration;
- study the dynamic response of the system to the different styles of trench motion;
- study the implications of these results on the kinematics of the Central Mediterranean subduction zone.

1.2 THESIS OUTLINE

The aim of this work is to study the effect of heterogeneities within the subducting plate on the dynamics of subduction. In particular, I study the motion of the trench for oceanic and continental subduction, first, separately, and, then, together in the same system to understand how they interact. This allows me to know what are

the effects of the different features included in the Central Mediterranean subduction model. In this Thesis, I describe the numerical method and the applied techniques in Chapter 2. Then, in Chapter 3, I analyse the trench motion for a purely oceanic subducting plate with 2D and 3D numerical models. In Chapter 4, I investigate the effect of continental subduction on trench migration in 2D and 3D domains. Moreover, I present the results of models with lateral density and thickness variations within the subducting plate. Finally, in Chapter 5, I develop a model that allows relating the main tectonic episodes of the Central Mediterranean with the evolution of the subduction process.

CHAPTER 2

Numerical modelling

2.1 MODELLING SUBDUCTION

Modelling subduction can be considered a problem of thermal and compositional convection: the motion of the plates is part of the mantle convection system, which is driven by internal buoyancy that derives from density variations. The main sources of density variations are thermal and compositional:

$$\Delta\rho(T,C) = \rho_0\left[\frac{\Delta\rho_c}{\rho_0} - \alpha(T - T_m)\right] \qquad 2.1$$

with symbols and values defined in Table 2.1. The thermal density difference arises from the thermal expansion α: the density increases with decreasing temperature. We can consider the plates as a thermal boundary layer within which the temperature changes from surface temperature to a reference temperature of the mantle. Thus, the plates are a cold, therefore, dense layer that has negative buoyancy and it leans to sink into the mantle. The compositional density variation is the effect of the different composition between the continental crust (ρ_c =2700 kg/m^3) and the mantle material (ρ_0 =3300 kg/m^3).

2.2 GOVERNING EQUATIONS

The thermal and composition convection in the mantle is governed by the conservation equations of mass, momentum, energy and composition. The mantle is treated as an incompressible viscous medium and the Boussinesq approximations are adopted (implying that the density differences are neglected except in the buoyancy term of the conservation of momentum equation).

For an incompressible fluid, the conservation of mass is described with a divergence-free velocity field:

$$\nabla \cdot u = 0 \qquad 2.2$$

The conservation of momentum is described with the Stokes equations and it represents the balance between pressure, viscous and body forces acting in the system:

$$\nabla p - \nabla \cdot \tau = \Delta \rho g \qquad 2.3$$

The conservation of energy describes the temperature field:

$$\frac{\partial T}{\partial t} + u \cdot \nabla T = k \nabla^2 T \qquad 2.4$$

The conservation of composition is described by a purely advective transport equation:

$$\frac{\partial C}{\partial t} + u \cdot \nabla C = 0 \qquad 2.5$$

This set of equations is non-dimensionalised by the following scaling expressions:

$$x = x'h \qquad t = t'h^2 / k \qquad u = u'k / h \qquad T = \Delta T\left(T' + T_0\right) \qquad \eta = \eta_0 \eta' \qquad 2.6$$

Dropping the primes, the non-dimensionalised set of equations became:

$$\nabla \cdot u = 0 \qquad 2.7$$

$$-\nabla p + \nabla \cdot \left(\eta\left(\nabla u + \nabla^T \boldsymbol{u}\right)\right) + \left(RaT + RbC\right)\boldsymbol{e}_z = 0 \qquad 2.8$$

$$\frac{\partial T}{\partial t} + u \cdot \nabla T = \nabla^2 T \qquad 2.9$$

$$\frac{\partial C}{\partial t} + u \cdot \nabla C = 0 \qquad 2.10$$

with the thermal Rayleigh number:

$$Ra = \frac{\alpha \rho_0 g \Delta T h^3}{k \eta_0} \qquad 2.11$$

and compositional Rayleigh number:

$$Rb = \frac{\delta \rho_c g h^3}{k \eta_0} \qquad 2.12$$

The Rayleigh numbers are controlling parameters of the vigour of convection.

2.3 THE FINITE ELEMENT METHOD (FEM)

The set of equations defined in 2.2 are solved with the Finite Element Method (FEM), using the parallel finite element code, Citcom [*Moresi and Solomatov*, 1995;

Zhong et al., 2000]. Conservation of mass, momentum and energy are solved using the Eulerian finite element technique, whereas, the transport of composition is performed with a Lagrangian tracer particle method (described in 2.4). The main difference between the Eulerian and the Lagrangian methods is the coordinates system: in the first case the flow field and the properties of the fluid are relative to fixed location in space, while, in the second case, the velocities of the particles of the flow are relative to the positions of the single particles.

The FEM is one of the most common methods to solve partial differential equations (PDE). The approach is to transform the PDE into an approximating system of ordinary differential equations that can be solved by using standard techniques. To do that, the model domain is discretized into a finite number of elements (mesh), within which the ordinary differential equations are solved using a fourth order Runge-Kutta integration. The big advantage of the FEM is that it can be used to solve problems with complex geometries, with non-homogeneous domains or with strong variations of material properties. For this reason it is suitable to model the subduction process, where all these features together create a complex system.

Following the algorithm described by *Moresi and Solomatov* [1995], the discrete form of Equations 2.7 and 2.8 (mass and momentum conservation) may be written in the form:

$$Au + Bp = f \qquad 2.13$$

$$B^T u = 0 \qquad 2.14$$

where A is the "stiffness" matrix, u is a vector of unknown velocities, B is the discrete gradient operator, p is a vector of unknown pressures and f is a vector composed by the body forces acting on the fluid. The coefficients of A, B and f are obtained using a standard finite element formulation with linear velocity and constant shape functions. Equation 2.13 can be transformed, if multiply by $B^T A^{-1}$ and use Equation 2.14 to eliminate the velocity unknowns:

$$B^T A^{-1} B p = B^T A^{-1} f \qquad 2.15$$

This is a form of the Uzawa algorithm and it is solved using an iterative conjugate gradient method. Equation 2.9 (conservation of energy) is solved using a standard Petrov-Galerkin method.

2.4 THE TRACERS METHOD

The Lagrangian tracer particle method is used to transport compositional properties through the domain in a time-dependent model [*Di Giuseppe et al.*, 2008; *van Hunen et al.*, 2002]. This method is applied to solve Equation 2.10. A large number of tracers (more than 40 per element) is initially emplaced with a uniform random special distribution in the model domain. These tracers are advected with the flow field at each timestep. The composition function, C, is a switch between two

end-member components: the continental crust (C=1) and the mantle material (C=0). At each timestep the interpolation of the compositional information is done per element and directly applied to the integration points, and vice versa. The resulting distribution of the tracers is used to determine the density of the material (continental crust vs. mantle density) and therefore, the buoyancy forces.

2.5 MODEL RHEOLOGY

Mantle and crustal rheology are key-controlling features of the dynamics of plate tectonics. Although there are still many uncertainties, laboratory measurements and analysis on postglacial rebound and geoid anomalies can help to constrain the rheological properties. This paragraph briefly describes the mantle and crustal rheology used in the models.

2.5.1 Mantle rheology

Several observations indicate that on a geological time scale the mantle deforms like a fluid. Although, at a first order, the mantle is often assumed to behave as a Newtonian fluid, it is more realistic to include a temperature and stress dependence on its viscosity. Laboratory studies on mantle minerals indicated that they are likely to deform with two main mechanisms: diffusion creep and dislocation creep. A general flow law for a single solid-state creep process in the mantle is [*Karato and Wu*, 1993]:

$$\dot{\varepsilon} = A\tau^n d^{-m} \exp\left[-\frac{E+pV}{RT}\right] \qquad 2.16$$

In the diffusion creep mechanism the deformation is limited by diffusion of atoms or vacancies through grains. In this case the stress dependence is linear (n=1), whereas there is a strong grain-size dependence (m=2-3). On the other hand, for the dislocation creep mechanism, the deformation is limited by the motion of dislocations through the grains, the stress dependence is nonlinear (n=3-5) and there is no grain size dependence (m=0). Estimates of the parameters of Equation 2.16 are given in [*Ranalli*, 1995] and the values used in this work are showed in Table 2.1.

From Equation 2.16 and knowing the viscosity and the strain rate are linked by this relationship:

$$\eta = \frac{\tau}{\dot{\varepsilon}} \qquad 2.17$$

the viscosity for a single creep mechanism can be defined as:

$$\eta = A^{-1/n}\dot{\varepsilon}^{(1-n)/n} d^{m/n} \exp\left[\frac{E + pV}{nRT}\right] \quad 2.18$$

For simplification and according to the Boussinesq approximation the activation volume V is assumed to be zero. Furthermore, the grain size parameter d and the factor A are put together in a pre-exponential constant:

$$A_D = A^{-1/n} d^{m/n} \quad 2.19$$

Given Equations 2.18 and 2.19 the viscosity can be described as:

$$\eta = A_D \dot{\varepsilon}^{(1-n)/n} \exp\left[\frac{E}{nRT}\right] \quad 2.20$$

Since both diffusion and dislocation creep act in the upper mantle, we define an effective viscosity η_{eff} that, at each point, is the minimum of the viscosity values derived from the mechanisms described above. This is a simplified expression for the composite rheology that uses the harmonic mean [*van den Berg et al.*, 1993].

Postglacial rebound models and geoid anomalies inversion are used to infer mantle viscosity. The estimates of viscosity that come from these analyses are independent on the laboratory measurements and they, thus, provide different tools to determine the effective viscosity of the mantle. Results from postglacial rebound models suggested a upper mantle viscosity of 3.6±1 x 10^{20} Pa s [*Lambeck and Johnston*, 1998]. Mantle viscosity value from geoid anomalies studies is slightly over 10^{20} Pa s [*Vermeersen et al.*, 1998]. In this work the reference mantle viscosity used is 10^{20} Pa s, but it is not a fixed value, since, as described above and in Equation 2.20, the viscosity is stress and temperature dependent.

2.5.2 Lithosphere rheology

The lithosphere can behave in two different modes: brittle and ductile (Figure 2.1). At depth, where the temperatures and pressures are high, the lithosphere is in the ductile regime. In this case, the same rheology of the mantle material is assumed (described in 2.5.1), although the viscous strength for crustal material is probably lower. In the models of Chapter 4, this difference is considered for the lower continental crust (see 4.4 for more details). While, near the surface, the lithosphere has a brittle behaviour and its viscosity is defined as:

$$\eta = \frac{\tau_y}{2\dot{\varepsilon}} \quad 2.21$$

with the yield stress is described as:

$$\tau_y = \min\left(\tau_0 + \mu p_0, \tau_{\max}\right) \quad 2.22$$

where $\tau_{\max}$ is the maximum yield stress and $\tau_0 + \mu p_0$ is the Byerlee's law [*Byerlee*, 1978], with τ_0 is the yield stress at the surface, μ is the friction coefficient

and p_0 is the lithostatic pressure. Values of τ_0, τ_{max} and μ are varied in the models and their range is showed in Table 2.2. The viscosity value from Equation 2.21 is considered to calculate the effective viscosity. Furthermore, given the strong temperature dependence on viscosity, to avoid non-realistic strength at the surface, where T=0, a maximum viscosity value η_{max} is imposed.

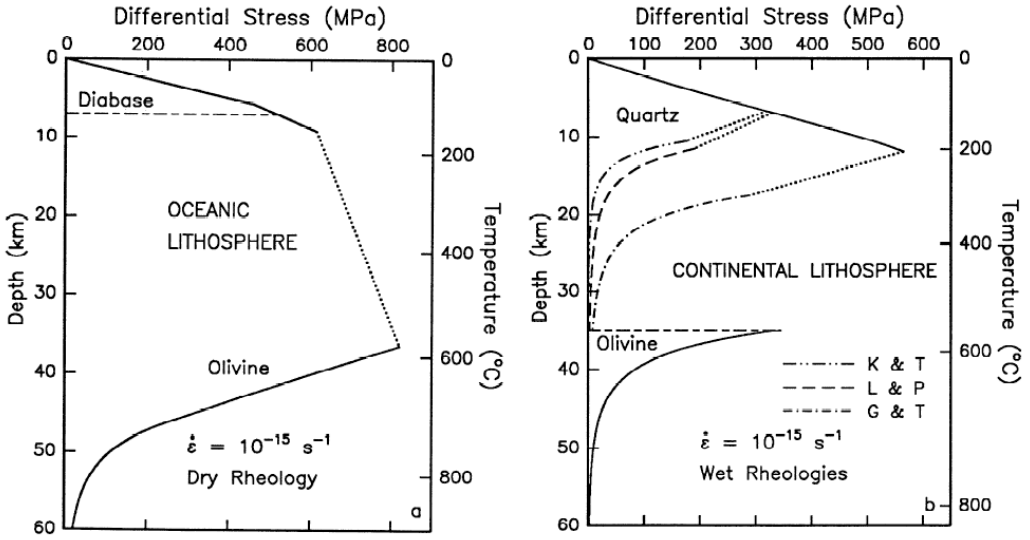

Figure 2.1 - Strength envelopes for oceanic and continental lithosphere. For oceanic lithosphere, the rheology of a dry olivine is used. For continental lithosphere, rheologies of wet quartzite proposed by different authors are used (see *Kohlstedt et al.* [1995] for details).

2.5.3 The subduction thrust fault and the mantle wedge

A strong deformation occurs between the plates, where large stresses are localized. In this zone, near the surface the strain is accommodated by earthquakes on major faults [*Kohlstedt et al.*, 1995] or shear localization [*Jin et al.*, 1998]. To model this feature and to enable decoupling between the convergent plates, a narrow low viscosity area is imposed. This weak zone is 20 km wide and extends down to 50 km, it has a viscosity value of 10^{20} Pa s and it has an arc-shape geometry with fixed radius of 0.8.

Furthermore, the slab dehydrates at a depth of 50-150 km: the subducting oceanic crust that has high water content, releases fluids because of the high temperature and pressure. In turn, the mantle above the slab can become weaker due to hydration and partial melting. To simulate this, without adding the complexity of de-hydration and melting, a weak mantle wedge is imposed. This weak mantle wedge starts at the base of the lithosphere up to 150 km, it is about 200 km wide and it has a viscosity value of 10^{20} Pa s.

Both the weak zone and the mantle wedge enable the decoupling between the plates. To study the trench migration in the subduction process, it is essential that

these features are able to move self-consistently with the dynamics of the system. In paragraph 2.7 the numerical technique used to allow this is described.

2.6 MODEL GEOMETRY AND BOUNDARY CONDITIONS

All the calculations are performed in a Cartesian geometry. The model domain has a depth of 660 km, which is the depth of the discontinuity between upper and lower mantle. The bottom boundary is assumed to be an impermeable barrier to flow, therefore, only the convection in the upper mantle is modelled and slabs are assumed to stagnate at the base of the upper mantle. Although it is known that large-scale convection in the whole mantle occurs and slabs are able to penetrate into the lower mantle, this assumption is motivated by the fact that there is a jump of few orders of magnitude in viscosity between upper and lower mantle that inhibits the flow between these two layers. The 660 km discontinuity is a major phase transition zone (from spinel to post-spinel) where the endothermic phase change [Ringwood and Irifune, 1988] generates positive buoyancy forces that keep the slab from directly penetrating into the lower mantle. The length and the width of the model domain are ranging from 2600 km to 3300 km.

In each model the initial setup is defined by a temperature field and, therefore, the thermal buoyancy creates a density contrast between the cold plates at surface and the hot mantle. Oceanic lithosphere follows the cooling half-space solution for a given plate age [*Turcotte and Schubert*, 2002] that increase from 0 Myr at the left boundary of the model domain to given age, varied in the models. While the continental lithosphere has an imposed maximum depth of 150 km. Initially, the slab extends down to about 300 km, to provide enough slab pull to drive subduction without imposing any external forces in a self-consistent model. The initial shape of the slab is consistent with data of curvature and dip angle from present-day observations of subduction zones [*Lallemand et al.*, 2005]. Since one of the main aims of this work is to study the effect of different types of variations (such as plate age, thickness and density) on subduction dynamics, the initial setup chosen for each study varies and it will be described in more details in each of the following chapters.

Thermal boundary conditions are: T=0° C at the surface and $T=T_m$ or $dT/dx=0$ (no heat conduction) along the other boundaries. Velocity boundary conditions are free-slip on all but the bottom boundary, where a no-slip condition is applied. A free-slip condition means that only the velocity component parallel to the boundary is allowed, whereas in a no-slip condition all the velocity components are null. The no-slip condition at the bottom of the model domain simulates the effect of the much higher viscosity of the lower mantle. All boundaries are closed, thus, no flow is allowed through them.

The finite element mesh is formed by rectangular elements. To have a better resolution at the convergent margin, where the narrow weak zone is imposed and there are strong viscosity contrasts in a relative small area, a mesh refinement is

applied. Element size ranges from 5x5 km^2 to 20x20 km^2 in the 2D models and 8x8x8 km^3 to 20x20x20 km^3 in the 3D models.

2.7 THE MOVING TRENCH

Trenches migrate in response to the dynamics of the subduction process. One of the main topics of this work is to study how geometrical, compositional and rheological parameters affect trench migration. For this reason, the possibility for the trench to move self-consistently with the system dynamics is an essential feature that has to be included in the models.

The following numerical technique is developed to model the trench migration. At each timestep the horizontal velocity v_{ov} of a point within the overriding plate and close (about 30 km) to the subducting plate is taken from the global model velocity field (Figure 2.2). This velocity is used to calculate the new position of the narrow weak zone between the plates:

$$x_1 = x_0 + v_{ov}\left(t_1 - t_0\right) \qquad 2.23$$

where x_0 and x_1 are the positions of the trench at time t_0 and t_1 respectively.

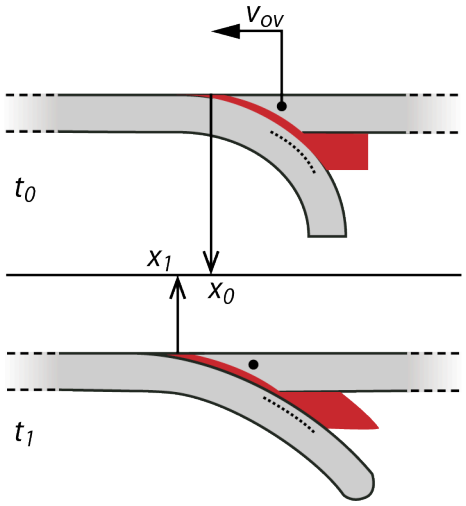

Figure 2.2 - Schematic cartoon of the technique applied to move the trench in a *xz* section from position x_0 at time t_0 to position x_1 at time t_1. The black dot shows where the velocity of the overriding plate (v_{ov}) is taken; the weak zones are represented with the red colour.

In the 3D calculations, this technique is extended to the *y*-dimension: the velocity of the overriding plate, used to move the trench, is calculated for each element of the mesh along the *y* direction close to the subducting plate (Figure 2.3). This method allows the trench to have lateral variations of velocities and positions in response to the geometrical, compositional and rheological variations of the model.

The shallow (0-50 km of depth) weak zone between the plates has a fixed shape, whereas the shape of the weak mantle wedge changes to follow the variations of the

dip of the slab during the model evolution. In this way the presence of the mantle wedge has no effect on the dynamics of subduction, except for helping the decoupling between the plates. The position of a set of a hundred tracers within the slab at a depth interval of 50-150 km is used to re-shape the mantle wedge according to the slab dip (Figure 2.2). Different positions to calculate the trench velocity and to infer the shape of slab have been tested to find the most suitable ones.

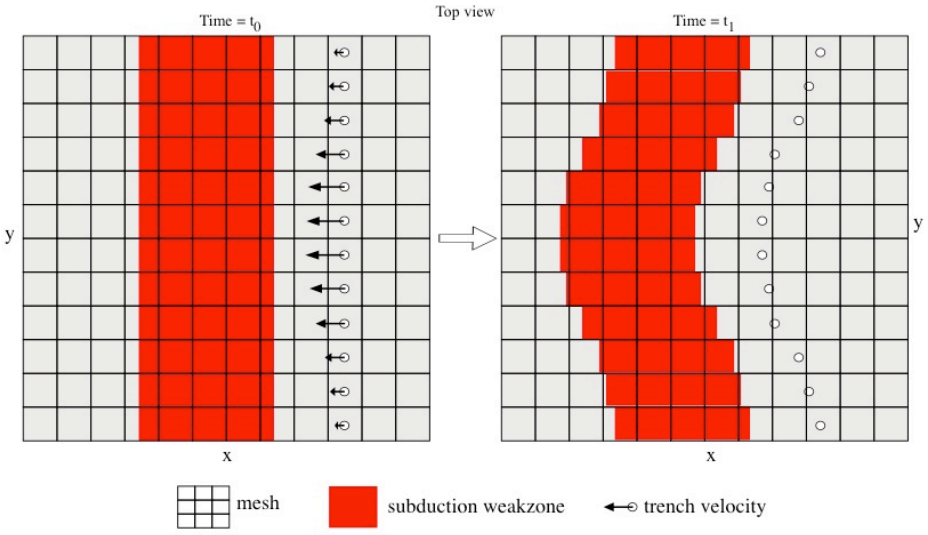

Figure 2.3 - Schematic cartoon of the technique applied to move the trench in the 3D models in a *xy* section from time t_0 to t_1. The white dots show where the velocity of the overriding plate is taken and the arrows indicate the magnitude of the velocity. The grid represents the computational mesh and the red colour indicates the weak zone.

2.8 TESTING NEW IMPLEMENTATIONS

In this work I use a step-by-step approach to study the subduction process. Starting from a simple model with a single plate sinking into the upper mantle, I progressively insert new features in the system to improve the model and, eventually, be able to develop a model of the Central Mediterranean subduction zone. The addition of each new feature needs to be tested in order to understand if the model outcomes are stable and consistent with natural data and previous models in the literature. For this reason, a set of several experiments is performed each time a complexity is added. Table 2.2 summarize all the models performed for this work, the explored parameters and the studied range of their values.

I performed several models related to the numerical techniques (marked with an asterisk in Table 2.2) to test, for instance, the code efficiency, the temperature and stress dependent viscosity and the new routines to move the trench. Although these

tests are essential, they are not part of the aims of this study and, therefore, they will not be discussed.

Parameters	***Symbols***	**Value**	**Unit**
Rheological pre-exponent	A_D	6.52 x 10^6	[Pa^{-n} s^{-1}]
Composition parameter	C	-	[-]
Grain size	d	-	[m]
Activation Energy	E	360	[kJ/mol]
Vertical unit vector	e_z	-	[-]
Gravital acceleration	g	9.8	[m/s^2]
Height of the domain	h	660	[km]
Thermal diffusivity	k	10^{-6}	[m^2/s]
Grain size exponent	m	-	[-]
Rheological power law exponent	n	1(diff. c.), 3.5(disl. c.)	[-]
Deviatoric pressure	p	-	[Pa]
Lithostatic pressure	p_0	-	[Pa]
Gas constant	R	8.3	[J/mol]
Thermal Rayleigh number	Ra	4.4 x 10^6	[-]
Compositional Rayleigh number	Rb	1.7 x 10^7	[-]
Temperature	T	-	[°C]
Time	t	-	[s]
Absolute tempertaure	T_{abs}	-	[K]
Reference temperature	T_m	1350	[°C]
Velocity	u	-	[m/s]
Activation volume	V	-	[m^3/mol]
Thermal expansion coefficient	α	3.5 x 10^{-5}	[K^{-1}]
Density variation	$\Delta\rho$	-	[kg/m^3]
Compositional density contrast	$\Delta\rho_c$	600	[kg/m^3]
Strain rate	$\dot{\varepsilon}$	-	[s^{-1}]
Viscosity	η	-	[Pa s]
Reference viscosity	η_0	10^{20}	[Pa s]
Maximum lithosphere viscosity	η_{max}	10^{22} - 10^{24}	[Pa s]
Friction Coefficient	μ	0 - 0.1	[-]
Reference density	ρ_0	3300	[kg/m^3]
Stress	σ	-	[Pa]
Deviatoric stress	τ	-	[MPa]
Surface yield stress	τ_0	40 - 200	[MPa]
Maximum yield stress	τ_{max}	200 - 400	[MPa]
Yield stress	τ_y	-	[MPa]

Table 2.1 - Symbols, units and default model parameters.

GOAL	EXPLORED PARAMETER	EXPLORED RANGE	N° of performed models
Testing code efficency*	Tracer density	200-800 tracers per unit	72
	Mesh resolution	from 5x5 to 20x20 km^2	
	N° processors	1-96	
	Box size	660x2640 - 660x4620 km^2	
	Slab curvature	0.6 - 0.8	
	Plates length	660-3000 km	
Temperature and stress dependent viscosity*	Mesh resolution	from 5x5 to 20x20 km^2	21
	μ_0, μ_{max}	20-200 MPa, 200-400 MPa	
	η_{max}	10^{23}-10^{24} Pa s	
	Activation energy	250-360 kJ/mol	
	Boundary conditions	T=T0 - T=Tm - open/close boundary	
	Box size	660x2640 - 660x4620 km^2	
Overriding plate*	μ_0, μ_{max}	20-200 MPa, 200-400 MPa	14
	η_{max}	10^{23}-10^{24} Pa s	
	Boundary conditions	T=T0 - T=Tm - free/no slip	
	Box size	660x2640 - 660x3300 km^2	
Moving trench:			
*Testing new routine**	Mesh resolution	from 5x5 to 20x20 km^2	52
	Mantle wedge depth	50-100 km	
	η mantle wedge	10^{19}-10^{21} Pa s	
	η weak zone	10^{19}-10^{21} Pa s	
	Box size	660x2640 - 660x3300 km^2	
	Slab curvature	0.6 - 0.8	
	Plates length	660-3000 km	
Free vs. fix trench (2D models)	μ_0, μ_{max}	20-200 MPa, 200-400 MPa	15
	η_{max}	10^{23}-10^{24} Pa s	
	Boundary conditions	T=T0 - T=Tm - free/no slip	
	Box size	660x2640 - 660x3300 km^2	
	Plates length	660-3000 km	
3D models	μ_0, μ_{max}	20-200 MPa, 200-400 MPa	9
	η_{max}	10^{23}-10^{24} Pa s	
	Plate age	30-60 Myr	
	Boundary conditions	T=T0 - T=Tm - free/no slip	
	Box size	660x2640x2640 - 660x3300x3300 km^3	

Continental subduction:			
2D models	μ	0-0.1	34
	η_{max}	10^{23}-10^{24} Pa s	
	Overriding plate	free/fix	
	Continental plateau length	660-1000 km	
	Box size	660x2640 - 660x3300 km^2	
	Plates length	1000-3000 km	
3D models	Plate age	50-80 Myr	10
	μ_0, μ_{max}	20-200 MPa, 200-400 MPa	
	η_{max}	10^{23}-10^{24} Pa s	
	Continental plateau width	330-1320 km	
	Box size	660x2640x2640 - 660x2640x3300 km^3	
Delamination	η lower crust	10^{19}-5x10^{21} Pa s	42
	η weak zone	10^{19}-5x10^{21} Pa s	
	η_{max}	4x10^{22}-10^{24} Pa s	
	Continental plateau length	200-1000 km	
	Box size	660x2640 - 660x3300 km^2	
	Plates length	1000-3000 km	
Mediterranean models	Overriding plate	free/fix	3
	η lower crust	10^{20}-10^{23} Pa s	

Table 2.2 - Performed models.

CHAPTER 3

Trench migration for oceanic subduction

3.1 INTRODUCTION

Many authors [e.g., *Bellahsen et al.*, 2005; *Christensen*, 1996; *Di Giuseppe et al.*, 2008; *Funiciello et al.*, 2003b; *Funiciello et al.*, 2008; *Gurnis and Hager*, 1988; *Stegman et al.*, 2006; *Zhong and Gurnis*, 1995] studied the motion of the trench and the subduction style modelling a single subducting plate sinking into the mantle. This kind of setup, which does not include an overriding plate and neither lateral plates, is commonly called 'free' subduction. These models focus on understanding the mechanisms that drives trench migration and how the geometrical and rheological characteristics of the lithosphere affected it. The main outcomes of these experiments are: (1) both retreating and advancing style are feasible and (2) the retreating mode is favoured for young (relatively thin and weak) plates (up to 70/80 Myr), low viscosity contrast or high density contrast between plate and mantle [*Di Giuseppe et al.*, 2008; *Faccenna et al.*, 2007a; *Funiciello et al.*, 2003b]. Other authors studied the oceanic subduction including the upper plate in their models focusing their attention on the variations of the slab dip and imposing a fixed position for the trench, [*Billen and Hirth*, 2007; *van Hunen et al.*, 2000]. Moreover, an other aspect of subduction is the associated mantle flow: many studies showed that the roll-back of the slab produces an increasing of pressure beneath it. This leads the mantle to flow around the edges of the slab in the horizontal plane (toroidal flow) [*Bellahsen et al.*, 2005; *Enns et al.*, 2005; *Faccenna et al.*, 2007b; *Funiciello et al.*, 2003a; *Piromallo et al.*, 2006; *Stegman et al.*, 2006]. Clearly, to investigate the toroidal component of the mantle flow, subduction has to be modelled in three dimensions. Furthermore, a 3D model allows to include lateral variations within the plates, such as thickness variations to simulate different ages of the oceanic lithosphere.

The assumption of the 'free' subduction models to not include the overriding plate might have an effect on the estimates of retreating velocities, since the subducting plate is surrounded by weak mantle material. *Capitanio et al.* [2010a] showed that the presence of an upper plate in the models has an important effect on

the dynamics of subduction. For this reason, in all the models of this study the overriding plate is included.

In this chapter, first, I investigate how the trench motion influences the dynamics of the system, comparing a 2D model with a static trench to one with a trench free to move self-consistently with the dynamics of the system. Then, I study the trench migration and the mantle flow induced by the evolution of subduction in a three-dimensional domain. Finally, I investigate the effect of the presence of lateral thickness variation within the subducting plate on the dynamics of the subduction process.

3.2 Model Setup

In this chapter numerical results of both 2D and 3D models of oceanic subduction are presented. In all models the computational domain is 660 km deep and has an aspect ratio of 1:5 (in 2D) and 1:4:4 (in 3D) (Figure 3.1). The initial temperature field of the subducting plate follows the cooling half-space solution for a given plate age [*Turcotte and Schubert*, 2002] and it increases from 0 Myr at the left boundary of the model domain to 30 Myr (in 2D) and to 30-50 Myr (in 3D). Therefore, older lithosphere is thicker, stronger and provides more slab pull than younger lithosphere. The oceanic overriding plate has a constant thickness of about 70 km.

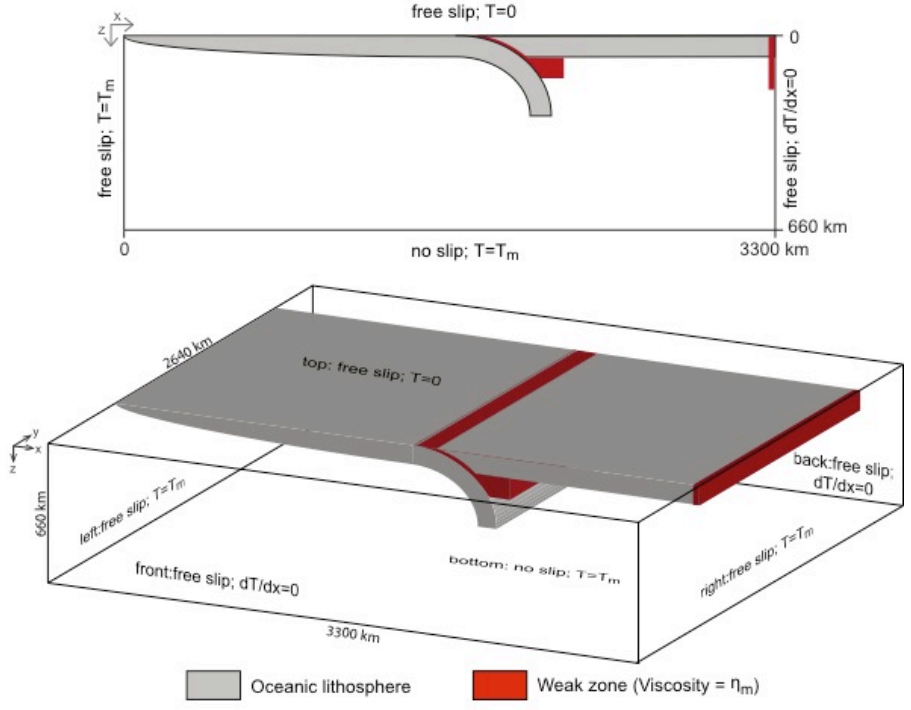

Figure 3.1 - Initial model setup with dimensions and mechanical and thermal boundary conditions. The model domain is 660 km deep and it has an aspect ratio of 1:5 or 1:4:4. The oceanic plates are represented in grey. Areas with an imposed low viscosity (i.e. the reference mantle viscosity) are outlined in red.

Thermal boundary conditions are: T=0°C at the surface, $T=T_m$ in the left and bottom boundary and in all the other boundaries no heat flux is allowed through them (dT/dx=0). No-slip condition is applied at the bottom boundary, whereas, free-slip condition is applied on all the others (Figure 3.1). A maximum viscosity of 10^{24} Pa s is imposed, to avoid non-realistic high strength at the surface. In all models, except for the one with a fixed trench, a low viscosity area ($\eta=10^{20}$ Pa s) is imposed at the top right corner to easily enable the motion of the overriding plate and, therefore, of the trench. Analyses on the effects of a fixed or free overriding plate on trench migration are performed in Chapter 4. In the 3D models the width of the plates is 1980 km and their motion is enabled by the presence of weak transform faults at y=330 km and y=2310 km with the same width and viscosity of the subduction fault. This allows for possible mantle flow around the slab edges and avoids boundary conditions on the sides of the domain to interact with the slab.

In an oceanic plate, the thin basaltic oceanic crust is buoyant for the first 30-40 km and, then, it is expected to transform in eclogite and have a density comparable to mantle material. Since its buoyancy effect is small, it is assumed to be negligible in the models. A rheology with a linear stress dependency is used for mantle and lithosphere material (see 2.5) and a constant yield stress of 200 MPa is applied (see Equation 2.22).

3.3 Effect of the Moving Trench: Free vs. Fixed trench

A 2D model with a fixed trench and one with a free trench are compared to investigate how the trench motion influences the dynamics of the system. Furthermore, the performed models are used to test the numerical technique applied to move the trench self-consistently with the system.

In both models the dynamics of subduction can be subdivided in three phases (Figure 3.2): 1) the sinking of the slab into the upper mantle, 2) the interaction of the slab with the 660 km discontinuity and 3) a nearly steady state condition, in which a invariable geometry and constant system velocities are achieved.

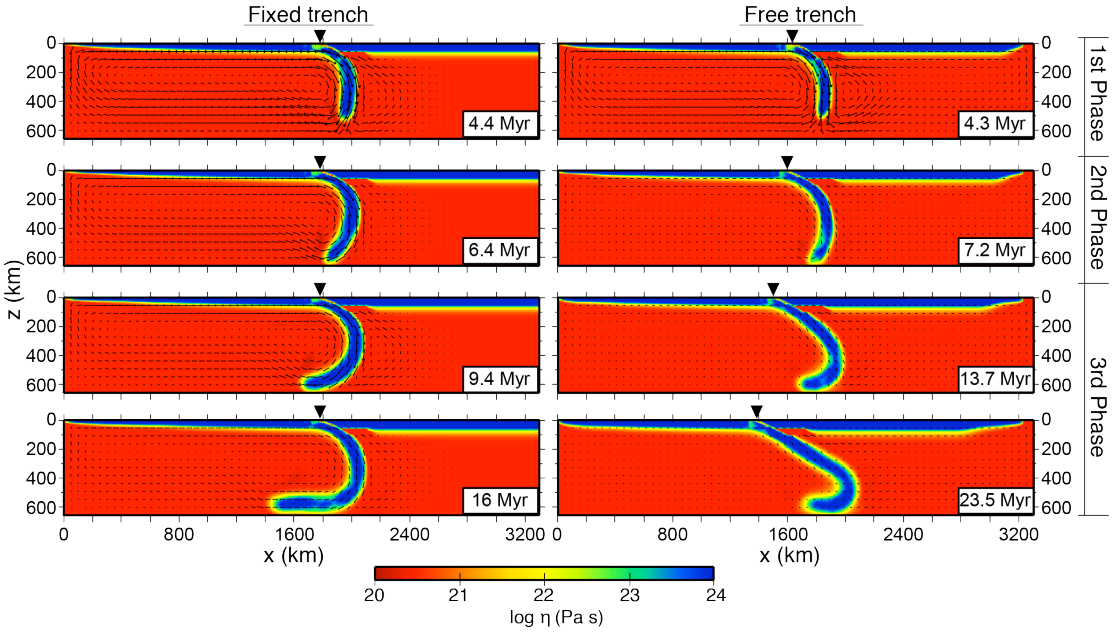

Figure 3.2 - Fixed vs. free trench model results: colours show the viscosity values and arrows indicate the velocity field. The black triangles show the trench position at each time step.

During the first phase, subduction velocity progressively increases because the more lithosphere subducts, the more pull is provided and, therefore, the faster the subducting plate moves (Figure 3.2). In this first phase, we observe a retreating style in the model with a free trench, with a maximum trench velocity of about 3 cm/y (Figure 3.3). In the second phase, the interaction between the slab and 660 km discontinuity causes a slowdown in the subduction process. This is also clear looking at the trench velocity: the minimum retreating velocity of 0.5 cm/y at about 7 Myr corresponds to the arrival of the slab at the bottom of the computational domain (Figure 3.2 and Figure 3.3). At this stage, we observe a strong difference in the geometry between the two models: where the trench is fixed, the slab is forced to keep the same shape it had at the interaction with the 660 km discontinuity, since not much deformation is allowed at shallow depths, and the steady state phase (phase 3) is soon reached (Figure 3.2). Whereas, in the model with a free trench, the slab unbends at depth and this is accommodated, at the surface, by the motion of the trench, leading to a flattening of the slab (Figure 3.2). In this model, after about 5 Myr since the beginning of phase 2, a constant retreating velocity of 1-1.5 cm/y is achieved (phase 3) (Figure 3.3).

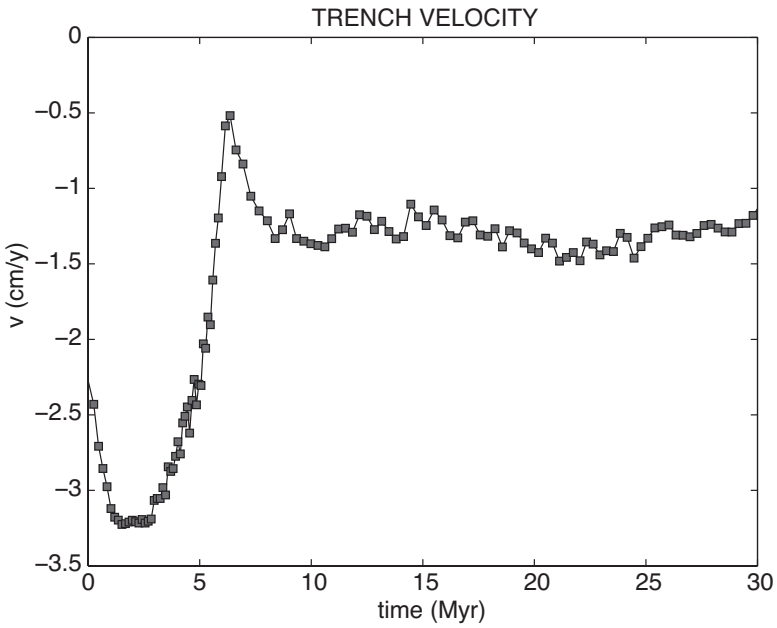

Figure 3.3 - Trench velocity of the 2D model with the free trench. Negative velocity is toward the subducting plate (retreating mode).

3.4 Trench retreat in 3D Models

Subduction of oceanic lithosphere with different ages (30, 40 and 50 Myr) is modelled in a three dimensional domain. In all the models the trench is free to move. The same three phases characterizing the 2D models described in 3.3 are observed in all the 3D models. The trench migrates backward with a progressively increasing velocity until the interaction with the 660 km discontinuity (Figure 3.4).

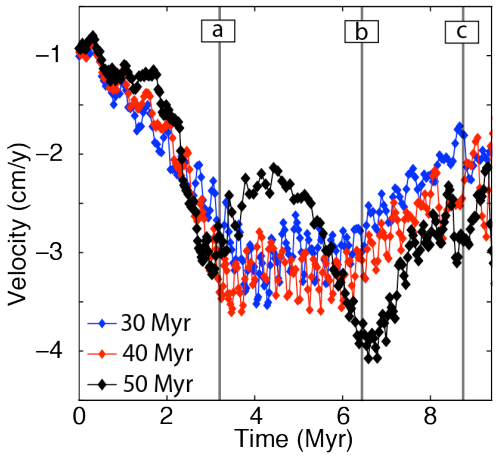

Figure 3.4 - Trench velocity of the 3D models with different plate age: 30 Myr (blue), 40 Myr (red) and 50 Myr (black). Negative velocity is toward the subducting plate. Lines a, b and c corresponds to the panels of Figure 3.5 with the results of the 50 Myr old plate model.

The flow field within the mantle, during the first phase, it is mostly characterized by a poloidal component: mantle material moves from behind to the front of the slab in *z*-plane (Figure 3.5a). Once the slab arrives at the bottom boundary, the poloidal component becomes null during the phase of interaction with the 660 km discontinuity and the mantle flows around the edges of the slab (toroidal flow) (Figure 3.5b). Although the toroidal flow occurs also during the first phase, it reaches the highest values of velocity after the interaction with the 660 km discontinuity. In particular, looking at the section *z*=330 km, we observe that the fastest toroidal flow occurs between 6.3 Myr and 8.3 Myr, corresponding to the fastest retreating of slab (Figure 3.6).

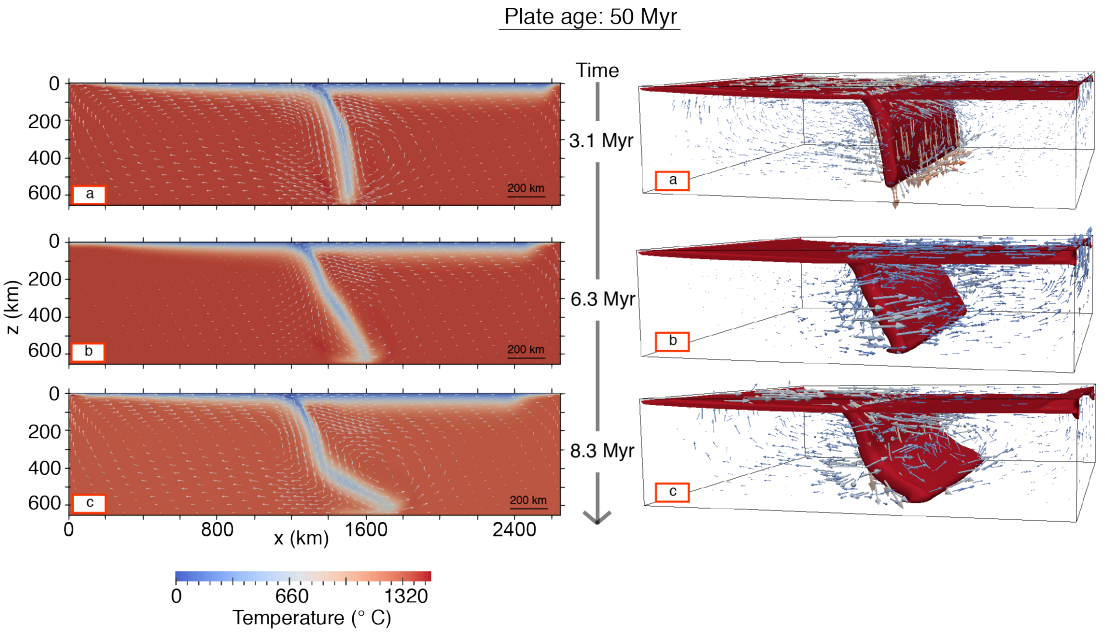

Figure 3.5 - Evolution of the model with the 50 Myr old plate. Column on the left shows the temperature field in the *y* =1320 km section (half of the domain). Column on the right shows 3D plots of the temperature isosurface of 1080° C. Arrows indicate the velocity field.

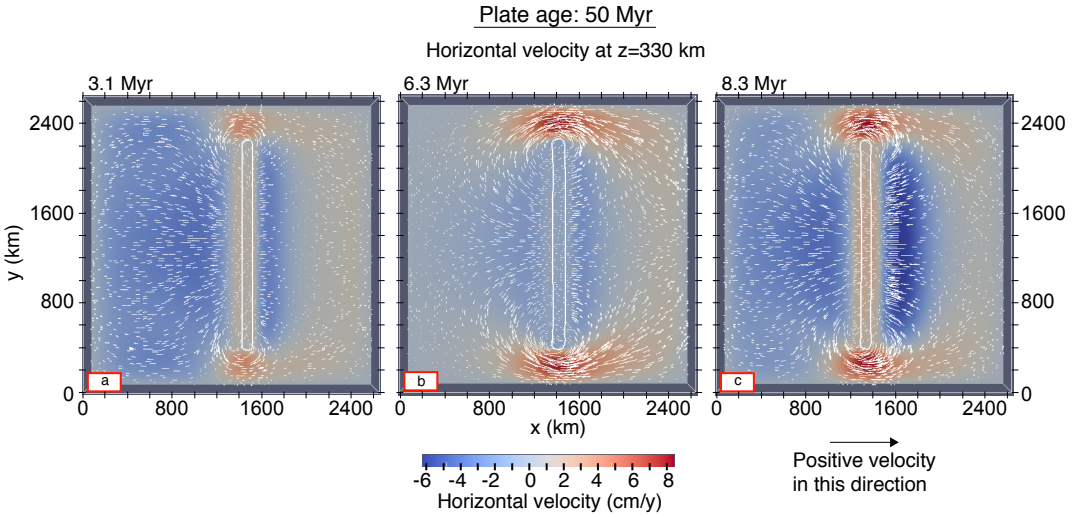

Figure 3.6 Mantle flow at the section z = 330 km for the model with the 50 Myr old plate at the time steps a (3.1 Myr), b (6.3 Myr) and c (8.3 Myr). Colours and arrows show the horizontal velocity field. Negative velocity (blue) is toward the subducting plate (on the left side in this model).

The unbending of the slab at depth occurs in all the models, but it has a larger effect on trench migration in the model with the oldest plate (50 Myr). In fact, although all the slabs arrive at the 660 km discontinuity with approximately the same dip, the depth at which they bend is different. In particular, the older the slab is, the shallower is the point where it bends (Figure 3.5 and Figure 3.7). This is due to the larger thickness, therefore a higher strength, of the oldest slab compared to the younger ones that makes more difficult its deformation. At this stage, a faster roll-back is observed in the model with the 50 Myr old plate with a maximum trench velocity of slightly more than 4 cm/y (Figure 3.4). Finally, in each model the last phase is characterized by a decreasing of the retreating velocity, since the trench moves towards younger and, therefore, thinner lithosphere.

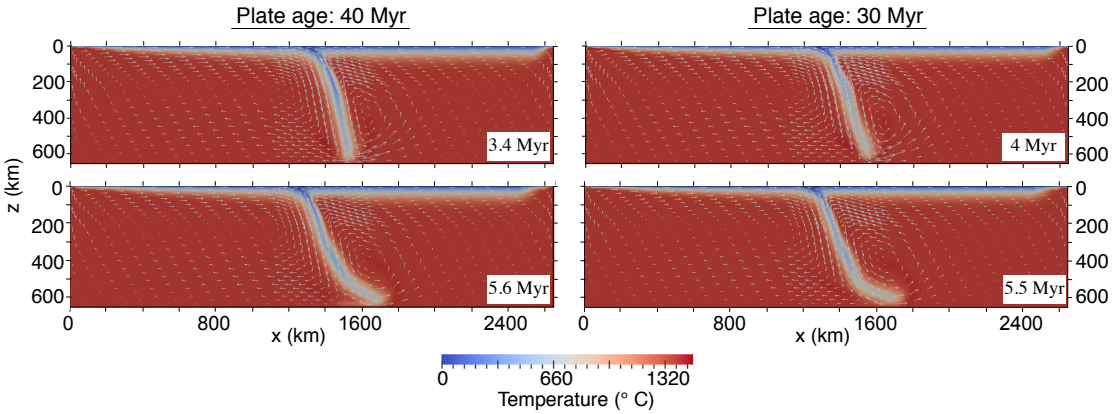

Figure 3.7 - Evolution of the models with the 40 Myr (left column) and 30 Myr (right column) old plate. Plots show the temperature field and arrows indicate the velocity field.

3.5 Lateral age variation: 3D Models

One of the main advantages of modelling the subduction process in a three dimensional domain is the possibility to include lateral heterogeneities. In this paragraph I will show the numerical results of a model in which the subducting plate has two different ages: half of the plate is 30 Myr old (P30), whereas, the other half is 50 Myr old (P50). The behaviour of a subducting oceanic plate in a 3D domain has been already shown in 3.4, so, in this part, I will focus on the effects of the lateral age variation on the dynamics of the system.

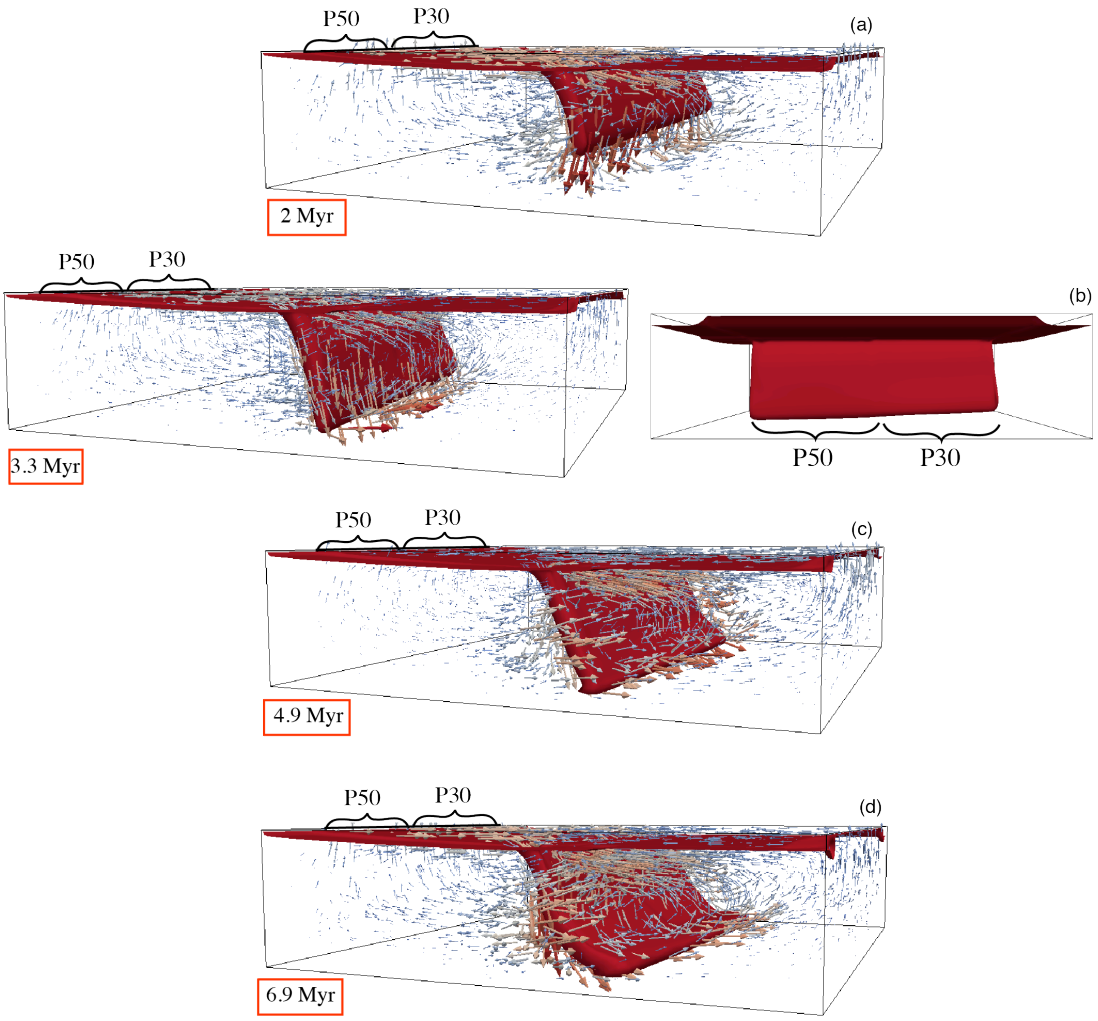

Figure 3.8 - Evolution of the model with lateral age variation. Plots show the temperature isosurface of 1080° C and arrows indicate the velocity field. The older part of the subducting plate (50 Myr) is indicated with P50, whereas the younger part (30 Myr) by P30. In the panels (b) also a front view of the subducting plate is showed to outline the tilting of the slab and the different timing of arrival at the 660 km discontinuity of P50 and P30.

The sinking of the slab does not occur with the same velocity along the whole plate, but is faster for the oldest part of the slab (Figure 3.8a). Accordingly, the 50 Myr old lithosphere reaches the 660 km discontinuity before the younger part of the plate. Moreover, in the first phase, P50 retreats more than P30, causing a tilting of the slab (Figure 3.8b and Figure 3.9a) and a curvature of the trench at the surface (Figure 3.9b). The decreasing of the system velocities (Figure 3.9a), due to the interaction of the whole plate with the bottom boundary, seems to re-equilibrate the system: the trench at 4.9 Myr from the beginning of subduction is less shifted than before (3.3 Myr) (Figure 3.9Figure 3.9). However, after few million years, the faster retreating of P50 starts again and the trench shape at surface shows a slight curvature (Figure 3.9b).

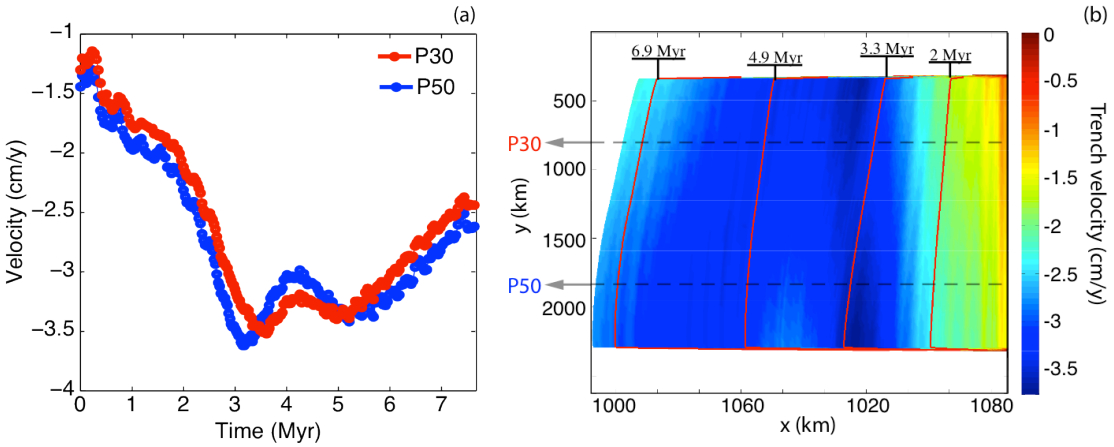

Figure 3.9 - (a) Trench velocity at two *y*-sections during the evolution of the model with lateral age variation of the two parts of the slab P30 (red) at y = 825 km and P50 at y = 1815 km (blue); (b) Plot show the trench position and shape during model evolution; colours show the trench velocity (negative toward the subducting plate) and the red lines outline the trench shape at the time steps showed in Figure 3.8.

3.6 Discussion and Concluding Remarks

The subduction of oceanic lithosphere is modelled in two- and three-dimensional domains with the aim at studying the trench migration during the models evolution. First, the effect of a trench free to move in the model is analysed. The numerical results show that the imposition of a fixed trench has a first-order effect on the dynamics of subduction. In fact, the resulting geometry of the slab is completely different: in the model with a fixed trench the slab has a backward-reclined shape, whereas, if the trench is free to move the slab is able to bend at depth and flattening at the surface. The low dip angle at shallow depths is the consequence of the fact that the subducting lithosphere is progressively younger and, therefore, more buoyant. Established the importance of trench migration in the numerical models, from now on all the models in this work will include this key-feature.

The results of the 2D and 3D models are in agreement with previous studies. The retreating style is expected when the subducting plate is younger than 70/80 Myr [*Di Giuseppe et al.*, 2008]. Furthermore, the obtained values of trench velocity (ranging from 0.5 to 4.3 cm/y) are consistent with the observed trench velocities of present-day subductions that vary from 0 to 12.3-14.5 cm/y with a mean of 2.2-3.9 cm/y (depending on the used reference frame) [*Funiciello et al.*, 2008]. The largest amount of retreating occurs in the model with the 50 Myr old subducting plate. This is due to the fact that the stresses needed to unbend an older and therefore, thicker and stronger, slab are larger and they propagate more, affecting also the deformation of the slab at shallow depths. In turn, the trench migrates to accommodate the deep deformation. The advancing mode is not obtained since only subduction of young oceanic lithosphere is modelled.

In the 3D models a large toroidal component is observed after the interaction with the 660 km discontinuity occurs. This is caused by the roll-back of the slab and, indeed, the highest velocities of the toroidal flow correspond to the fastest backward motion of the trench. Many numerical [e.g., *Enns et al.*, 2005; *Piromallo et al.*, 2006; *Stegman et al.*, 2006] and analogue models [e.g., *Bellahsen et al.*, 2005; *Funiciello et al.*, 2003a] found the same mantle behaviour as a consequence of slab roll-back. Evidences of this kind of local flow pattern in the mantle are provided by geochemical and seismological studies. For example, in the southern Tyrrhenian region, the amount of mantle material flowing inside the back-arc region has been large enough to change the composition of the erupted magmas [*Faccenna et al.*, 2007b]. Moreover, seismological analyses in this area showed that the orientation of the splitting anisotropy matches with this kind of local mantle flow.

Accordingly with the difference in retreating velocity found for models with different plate age, a direct consequence of including lateral age variations within the subducting plate is the differentiate trench motion. Indeed, results from model described in 3.5 show that the trench does not remain straight during the evolution of subduction, but it curves to accommodate the different velocities. This trench curvature is only slight since the difference in plate age is not so large. Moreover, the high strength of the lithosphere ($\eta_{max}=10^{24}$ Pa s) limits the deformation of the overriding plate, which is required for trench deformation.

CHAPTER 4

Trench migration for continental subduction

4.1 INTRODUCTION

4.1.1 Continental collision scenarios

Slab pull caused by the negative buoyancy of subducting lithosphere represents the main driving contribution for plate motion: [e.g., *Chapple and Tullis*, 1977; *Conrad and Lithgow-Bertelloni*, 2002; *Elsasser*, 1969; *Forsyth and Uyeda*, 1975]. When continental lithosphere enters the subduction zone, its positive buoyancy acts as a resisting force to sinking and, therefore, leads to a slowdown, and eventually to the end of subduction [*Cloos*, 1993]. After collision three possible scenarios may occur: (1) continental crustal material arrives at the trench and subducts together with the lithospheric mantle [e.g., *Conrad and Lithgow-Bertelloni*, 2002; *Ranalli et al.*, 2000; *Regard et al.*, 2003; *Toussaint et al.*, 2004]; (2) part of the continental buoyant crust is delaminated from the lithospheric mantle and accreted to the overriding plate, allowing continuation of plate convergence (delamination) [e.g., *Bird*, 1979; *Chemenda et al.*, 1996; *Cloos*, 1993; *Kerr and Tarney*, 2005] or (3) the slab breaks off as a consequences of tensile stress from the pull of the sinking oceanic lithosphere in the mantle connected to the continental part of the plate [*Davies and Von Blanckenburg*, 1995; *Wortel and Spakman*, 1992] (Figure 4.1). Which scenario takes place depends on several factors including convergence rate, thickness, rheological and physical composition and thermal structure of the continental lithosphere [*van den Beukel and Wortel*, 1987]. *De Franco et al*. [2008] suggested that the geometry of the incoming continental plate, the tectonic setting, the rheology and the length of the sinking oceanic plate controls whether the incoming crust subducts entirely, separates partially or entirely from the lithospheric mantle or blocks the trench, likely leading to slab break-off.

Although continental collision eventually leads to the cessation of subduction, the amount or even direction of associated trench migration is not well understood. *Royden* [1993] proposed two end-member classes of continental subduction

boundary: the retreating and the advancing style. A brief description of these two modes is presented in the following paragraphs.

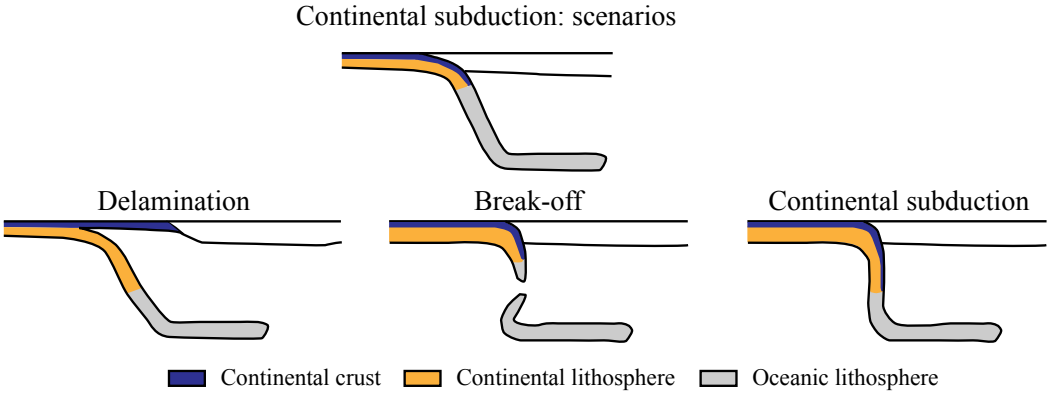

Figure 4.1 - Schematic cartoon of different continental subduction scenarios: delamination, break-off and continental subduction.

4.1.1.1 The advancing mode

In the advancing subduction systems, hundreds of kilometers of continental lithosphere subducts without crustal delamination [*Royden*, 1993]. The morphology of the subducted slab inferred from tomographic images provides evidence of trench advancing in continental collision zones like the India-Eurasia system [*Replumaz et al.*, 2010; *Replumaz et al.*, 2004] and Arabia-Eurasia [*Hafkenscheid et al.*, 2006].

The advancing motion is often explained with far field stresses related to global plate motion that push the plates and force the trench to migrate towards the overriding plate. For example, to explain Indian indentation rates the ridge push of Indian ocean [*Chemenda et al.*, 2000], the presence of the Réunion plume [*Cande and Stegman*, 2011] or the pull of adjacent slabs [*Li et al.*, 2008] has been invoked. *Capitanio et al*. [2010b] suggested that in the India-Eurasia collisional system an imbalance between ridge push and slab pull can develop and cause trench advance and indentation. To explain the advancing of India into the Arabia-Eurasia system [*Becker and Faccenna*, 2011] proposed that mantle drag exerted on the base of the lithosphere by a large-scale mantle flow component with an active upwelling component is likely the main cause for the ongoing indentation.

4.1.1.2 The retreating mode: delamination

In the delamination process, the lithospheric mantle detaches from the buoyant continental crust and it keeps subducting into the mantle. In this scenario, the remaining slab, formed by the lithospheric mantle, retreats away from the suture zone, leaving a thin layer of crust between the suture zone and the delamination front. [*Royden*, 1993]. This causes an extensional regime within the overriding plate, which has been observed in subduction zones as the Apennines [*Channell and Mareschal*, 1989] and the Carpathians [*Houseman and Gemmer*, 2007].

According to *Meissner and Mooney* [1998] and *Jull and Kelemen* [2001] the basic driving force for delamination is the negative buoyancy of the continental lower crust and subcrustal lithosphere. *Jull and Kelemen* [2001] show that a lower crust with a low viscosity playing as a decoupling level is necessary to obtain lithospheric mantle root removal under compressive deformation.

4.1.2 Continental subduction models

Several studies on continental subduction discuss the dynamics of slab break-off [e.g., *Davies and Von Blanckenburg*, 1995; *De Franco et al.*, 2008; *Duretz et al.*, 2011; *Regard et al.*, 2003; *Wong A Ton and Wortel*, 1997; *Yoshioka and Wortel*, 1995]. In many areas where continental collision occurs, seismic tomography has revealed the presence of gaps in the subducting lithosphere, interpreted as evidence of detached lithosphere within the slab (e.g., Mediterranean, Carpathians, eastern Anatolia) [*Carminati et al.*, 1998; *Hafkenscheid et al.*, 2006; *Lei and Zhao*, 2007; *Wortel and Spakman*, 2000]. Other suggestions of slab detachment have been provided by geochemical studies of magmatism in collision zones [*Ferrari*, 2004; *Keskin*, 2003; *Qin et al.*, 2008].

Numerical models suggest that break-off can occur at the depth interval of 20-380 km and with different timing, from 2 to 40 Myr, controlled by changing parameters such as plate age, convergence velocity and rheology of the system [*Andrews and Billen*, 2009; *Duretz et al.*, 2011; *Gerya et al.*, 2004; *van Hunen and Allen*, 2011; *Wong A Ton and Wortel*, 1997]. *Van Hunen and Allen* [2011] illustrated how, due to the difference in necking in two dimensional (2-D) and three-dimensional (3-D), break-off has an intrinsic small preference to start as a window within the slab interior, rather than as a tear at the slab edge.

Laboratory models by *Regard et al.* [2003] showed that the amount of continental material that can be subducted increases with the slab-pull force exerted by the oceanic subducted lithosphere and that two different modes of slab deformation (i.e. slab break-off or development of a viscous instability) can occur as a function of the balance between total pull and strength of the slab.

These models assume a uniform continental crust and, therefore, do not take into account the possible scenario of delamination. *Gogus et al.* [2011] performed laboratory experiments of oceanic subduction followed by continental collision, modelling the lower crust as a low viscosity layer. They suggest that continental mantle lithosphere delamination may develop following the transition from retreating oceanic subduction to collision and that low convergence velocities facilitate the occurrence of delamination. Using temperature-dependent numerical experiments, *Morency and Doin* [2004] suggest that delamination can only occur when Moho temperatures exceed 800°C. This results in a mechanical decoupling between the crust and mantle lithosphere along the weak lower crust [*Bird*, 1979; *Meissner and Mooney*, 1998; *Ranalli et al.*, 2000]. In numerical experiments with a brittle-viscous

crust and mantle lithosphere reaching effective viscosities of 10^{23} Pa s, a viscosity of $5x10^{19}$ Pa s of the (hot) lower crust effectively decouples the lithosphere [*Göğüş and Pysklywec*, 2008a; b].

An important aspect of continental collision is how plates deform. Many analogue laboratory models of continental collision show that a subducting plate will deform internally only if the force distribution varies laterally along the subduction zone, e.g. by the asymmetrical entrance of continental material along the trench [*Bellahsen et al.*, 2003; *Faccenna et al.*, 2006; *Regard et al.*, 2005]. The along-trench variation of the subducting plate plays an important role in convergent margin deformation, and is often invoked to explain the indenter-like geometry of plate boundaries (e.g., the India-Eurasia plate boundary). Hence, plate deformation and trench migration play a critical role in a continental collision system.

In this chapter, I study the continental subduction and its influence on the geometry and kinematics of the process. First, I use 2D geodynamical numerical models to investigate the dynamic behaviour of trench during continental collision without external forces, i.e. driven entirely by the changes in the net internal driving force direction and magnitude. I explore the robustness of these results with a parametric study where geometrical and rheological constraints of the system are systematically changed in order to define their effect on the kinematics of continental collision. In these models the continental crust is modelled as a uniform layer.

Then, I study the feasibility of the delamination process by investigating the effect of a weak lower crust on the evolution of continental subduction. The main issue is: which is the most suitable configuration of the continental crust to favour delamination and which is, on the other hand, the one that favours slab detachment? For this purpose, I perform a parametric study by changing the viscosity profile of the continent in 2D models.

Finally, a set of ten 3D models are presented of continental subduction with different geometry and position of the continental plateau to understand how lateral density and thickness variations affect the system dynamics. I present the results of two models that are representative of the whole set of experiments: a model with a uniform continental crust and one with a layered crust. These models are also useful to investigate how the whole system responds to the occurrence of break-off and delamination.

4.2 Model Setup

In this chapter numerical results of both 2D and 3D models of oceanic subduction are presented. In all models the computational domain is 660 km deep and has an aspect ratio of 1:5 (in 2D) and 1:5:4 (in 3D). The closure of an ocean basin and subsequent continental collision is modelled. In the initial setup the incoming plate

consists of a subducting oceanic lithosphere with a continental block initially about 500 km from the trench (Figure 4.2). The overriding plate is entirely continental. The initial temperature field for the oceanic lithosphere is calculated following the half-space cooling solution for a 50-Myr old plate [*Turcotte and Schubert*, 2002]. For the continental lithosphere, temperature extends linearly from 0° C at the surface to the mantle reference temperature at 150 km depth. A 40-km deep continental crust is characterized by positive buoyancy (the density difference between the continental crust and the mantle material is 600 kg/m^3), which creates a resisting force to subduction when the continental block inside the subducting plate arrives at the trench.

The top boundary has a fixed temperature of 0°C, whereas the other boundaries have a fixed mantle temperature T_m=1350°C. Velocity boundary conditions are free-slip on all but the bottom boundary, where a no-slip condition is applied.

In the 3D models the width of the plates is 1980 km and their motion is enable by the presence of weak transform faults at y=330 km and y=2310 km with the same width and viscosity of the subduction fault. This allows for possible mantle flow around the slab edges and avoids boundary conditions on the sides of the domain to interact with the slab. The continental plateau is 660 km wide and its position is in the middle of the subducting plate. A maximum viscosity value is set to 10^{23} Pa s.

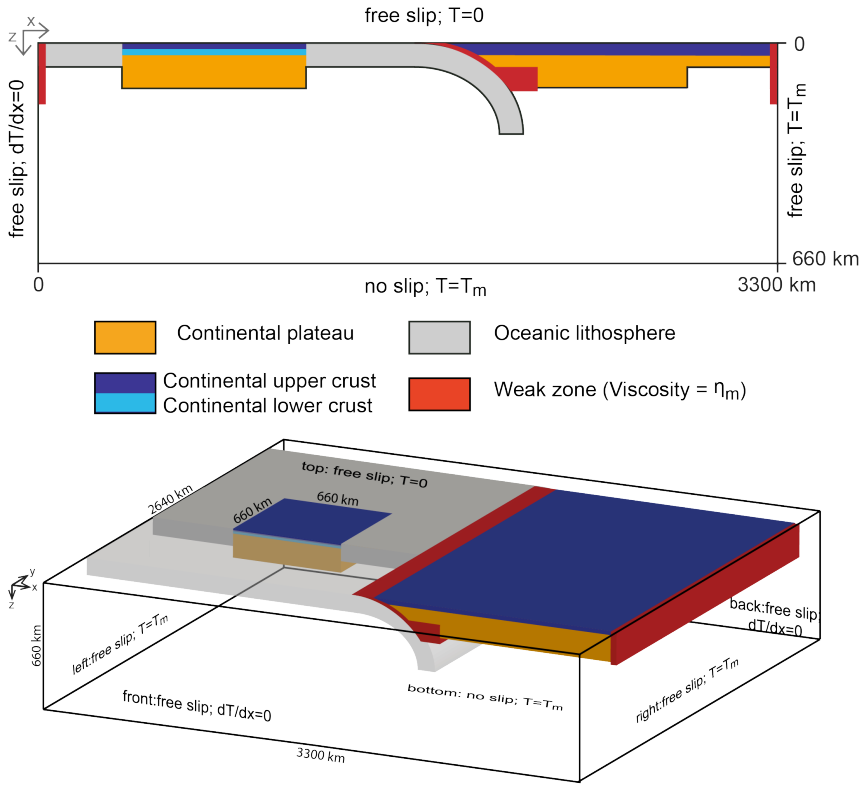

Figure 4.2 - Initial model setup with dimensions and mechanical and thermal boundary conditions. The model domain is 660 km deep and it has an aspect ratio of 1:5 or 1:5:4. The oceanic lithosphere is represented in grey, the continental parts are modelled with a thick lithosphere (yellow) and a 40 km buoyant crust (blue for the upper crust and light blue for the lower crust). Areas with an imposed low viscosity (i.e. the reference mantle viscosity) are outlined in red.

4.3 MODELLING RESULTS

4.3.1 Uniform Continental Crust

We performed two sets of model calculations. In the first set, we investigate the effect of the presence of buoyant continental lithosphere on trench motion. All models have the same initial geometry setup. Given the sensitivity of results to plate strength, differences among the models concentrate on two rheological parameters: the maximum viscosity of the lithosphere (η_{max}) and the friction coefficient μ. η_{max} varies between 10^{23} and 10^{24} Pa s, whereas μ varies between 0 and 0.1. In models with μ=0 the maximum yield stress τ_{max} and the surface yield stress τ_0 are both 200 MPa, whereas, in models with μ=0.1, τ_0=40 MPa and τ_{max} =400 MPa (Table 4.1). All of these parameters have a strong influence on the subduction dynamics because they control the strength of the lithosphere and, therefore, its capability to deform and bend. We compare these models with a similar set of models with a purely oceanic subducting plate, i.e. by replacing the continental block with oceanic lithosphere, which affects average density and thermal thickness.

Model	Max η [Pa s]	μ	τ_0 (MPa)	τ_{max} (MPa)	Subducting plate	Overriding plate
C1	10^{23}	0	200	200	continental	free
C2	10^{23}	0,1	40	400	continental	free
C3	10^{24}	0	200	200	continental	free
C4	10^{24}	0,1	40	400	continental	free
C5	10^{23}	0	200	200	continental	fix
C6	10^{23}	0,1	40	400	continental	fix
C7	10^{24}	0	200	200	continental	fix
C8	10^{24}	0,1	40	400	continental	fix
O1	10^{23}	0	200	200	oceanic	free
O2	10^{23}	0,1	40	400	oceanic	free
O3	10^{24}	0	200	200	oceanic	free
O4	10^{24}	0,1	40	400	oceanic	free

Table 4.1 - Summary of the models used in this parametric study (4.3.1).

The reference continental model C1 (Figure 4.3) has a maximum viscosity value of 10^{23} Pa s and depth-independent yield strength (i.e., μ=0). The model dynamics can be subdivided in 4 phases: 1) the sinking of the slab into the upper mantle, 2) the unbending of the slab due to its interaction with the 660 km discontinuity, 3) the arrival of the continental plateau at the subduction zone and 4) the necking and break-off of the slab at depth. In the first phase the trench retreats (Figure 4.3 and Figure 4.4) and its velocity decreases while the slab approaches the 660 km discontinuity. Afterwards, during phase 2, because of the unbending of the slab at depth, the retreating velocity increases in order to accommodate the deep deformation (Figure 4.3 and Figure 4.4). After about 3.5 Myr from the beginning of the process, the continental plate reaches the zone where the slab needs to bend to enter the trench (phase 3; Figure 4.4b). At this stage the trench velocity decreases until, at about 5 Myr, the continent arrives at the subduction zone, and the trench starts to advance (Figure 4.4). At this point the buoyancy of the continental crust chokes the subduction process, which dramatically slows it down. After about 7 Myr since the arrival of the continent at the trench (see Fig. 2 panel 12.6 Myr), the slab starts showing the first indications of necking and eventually it breaks because of the interaction of the two opposite forces: the pull of the oceanic slab at the depth and the buoyancy of the shallow continental crust (phase 4). During this last phase the trench motion slightly increases its velocity for a short period and then it completely stops (Figure 4.4). The break-off occurs after about 13 Myr from the collision and the continent reaches its maximum depth of ~160 km. The amount of trench advancing is about 100 km from 5 to 22 Myr (Figure 4.4).

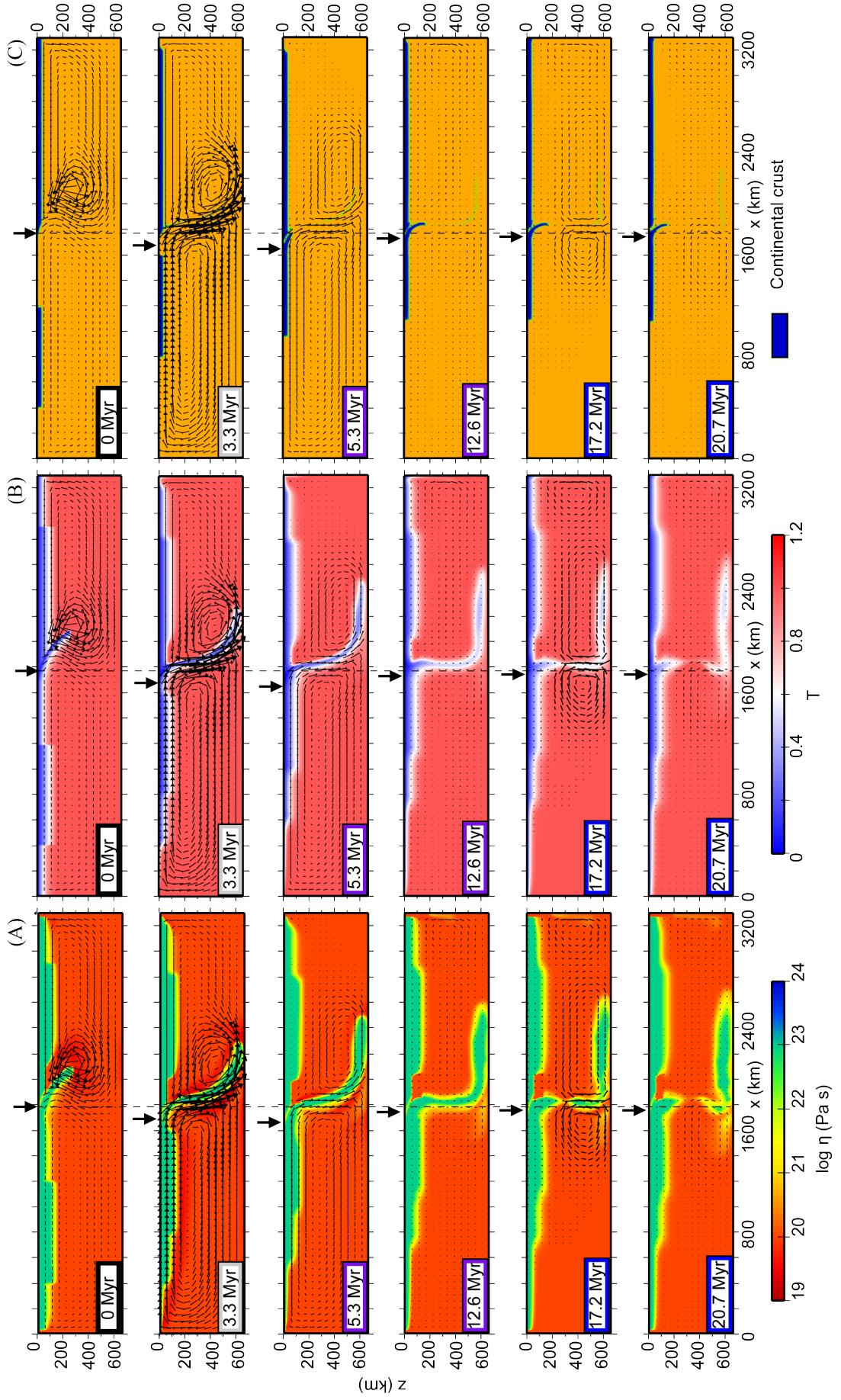
(A)
(B)
(C)
0 Myr
3.3 Myr
5.3 Myr
12.6 Myr
17.2 Myr
20.7 Myr
z (km)
x (km)
log η (Pa s)
T
Continental crust

Figure 4.3 - Evolution of the reference model C1: column (A) viscosity plots, (B) temperature plots and (C) compositional plots. Arrows indicate the trench position at each timestep; dotted lines show the trench position at the beginning of the model. Square colours indicate the 3 different subduction phases: black, grey and purple respectively.

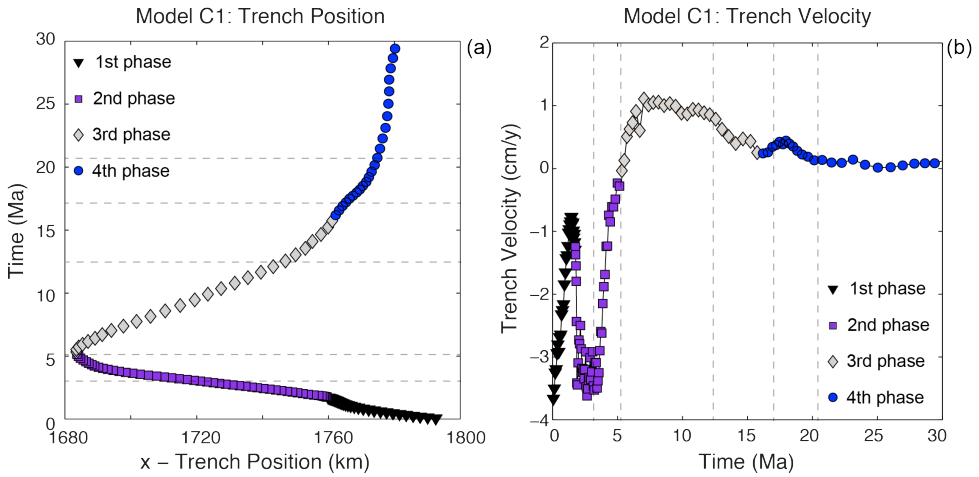

Figure 4.4 - Model C1: trench (a) migration and (b) velocity during model evolution. Colours indicate the three different subduction phases. Dashed lines correspond to panels in Figure 4.3.

Results from the continental model (C4) with an increased maximum viscosity value of 10^{24} Pa s and μ=0.1 are shown in Figs. 4 and 5 Although, in comparison to model C1, the cold parts of the slabs becomes stronger, material near the surface has a reduced strength due to the depth-dependent yield strength. Compared to C1 the amount of retreat in the first phases of subduction is larger. This is mostly due to the low yield strength at the surface, which reduces the effective viscosity of the plate in the bending zone where stresses are higher. The collision occurs after about 7 Myr since subduction started and the trench begins to advance (Figure 4.5 and Figure 4.6). The slab starts necking at about 16 Myr and it breaks after 25 Myr. The trench advancing is clearly accelerated during this phase (Figure 4.6). The continental crust arrives at a depth of almost 200 km (Figure 4.5). Compared to C1, it takes longer for the slab to break because the higher maximum viscosity makes the slab stronger. Moreover, the continental crust arrives about 40 km deeper compared to C1, mostly because the lower yield strength at the surface allows for easier bending and, therefore, favours the subduction. In this model the amount of advancing is about 220 km in 20 Myr (Figure 4.6).

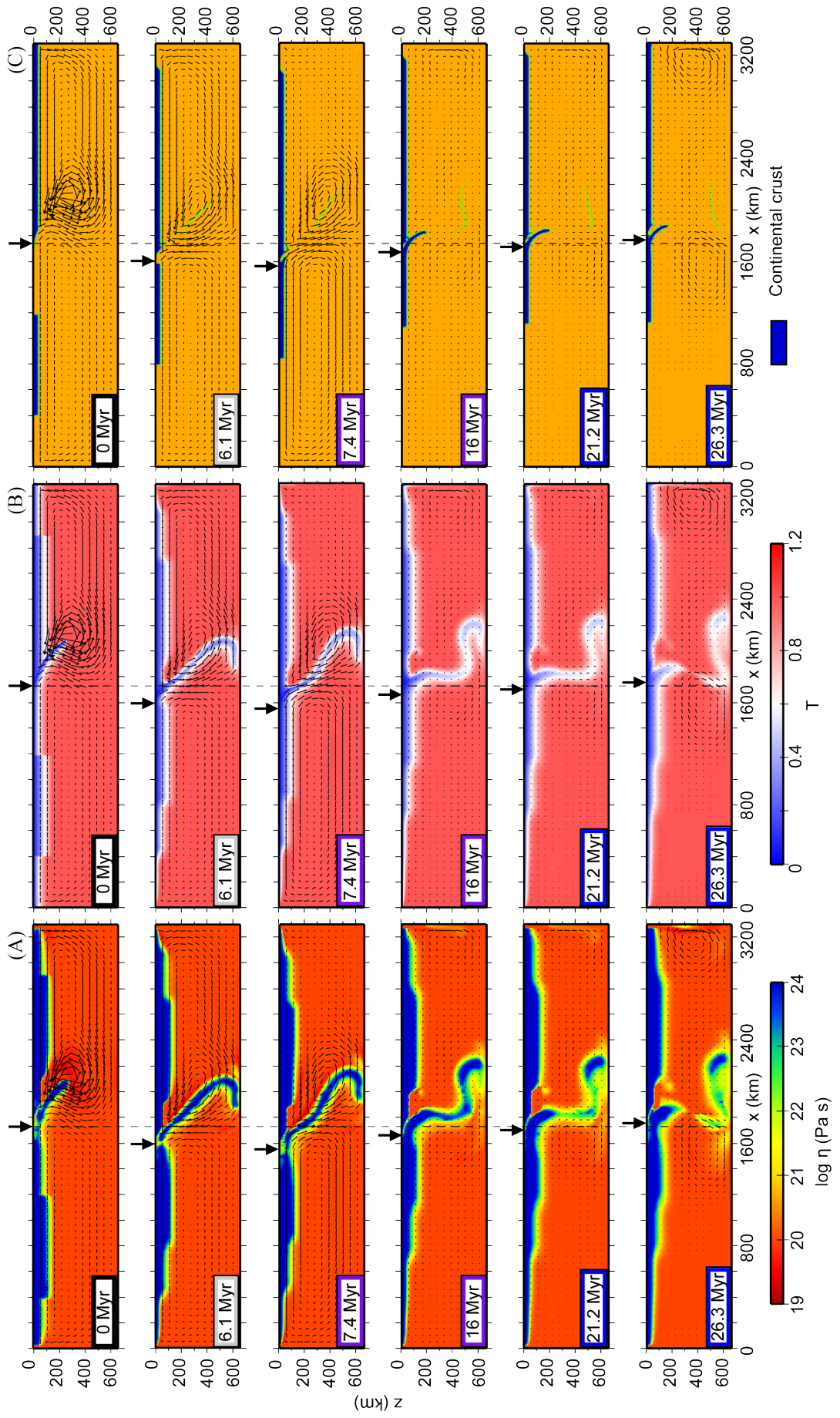
(A)
(B)
(C)
0 Myr
6.1 Myr
7.4 Myr
16 Myr
21.2 Myr
26.3 Myr
z (km)
x (km)
log η (Pa s)
T
Continental crust

Figure 4.5 - Evolution of the model C4: column (A) viscosity plots, (B) temperature plots and (C) compositional plots. Arrows indicate the trench position at each timestep; dotted lines show the trench position at the beginning of the model.

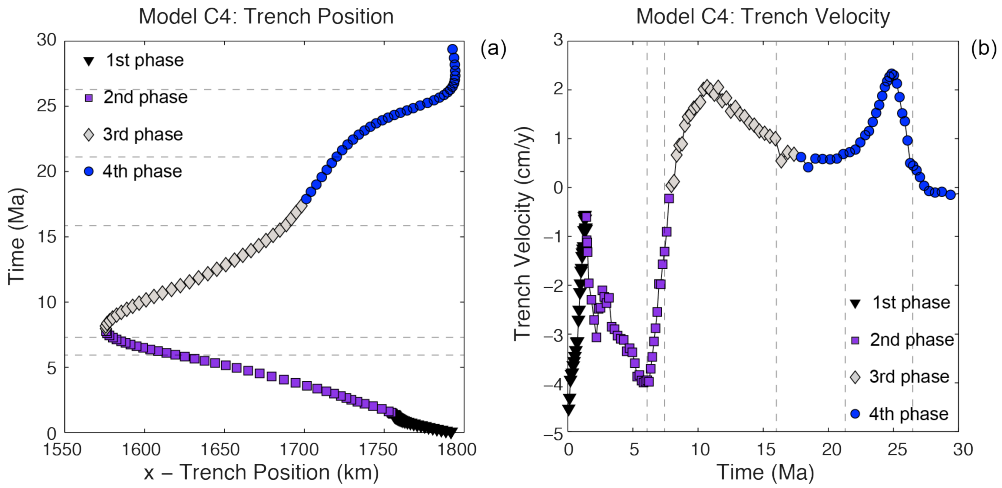

Figure 4.6 - Model C4: trench (a) migration and (b) trench velocity during model evolution. Colours indicate the three different subduction phases. Dashed lines correspond to panels in Figure 4.5

When the reference model C1 is compared to model O1, with a purely oceanic lithosphere but otherwise the same rheological parameters of C1, significant differences are evident (Figure 4.7). In the first two phases of subduction (sinking of the slab and unbending) the dynamics of the system is the same. Figure 4.7d-e shows that trench velocities and positions are almost identical until about 4 Myr. In model C1, 4 Myr corresponds to the arrival of the continental plateau to the bending zone close to the trench, whereas, in model O1 the system reaches the steady-state condition of retreating. Comparing O1 with all the other oceanic subducting plate models (Figure 4.8) we observe that the amount of retreat and trench velocity slightly change because of the difference in the slab strength due to the variations of the rheological parameters, but the overall subduction dynamics remains unchanged.

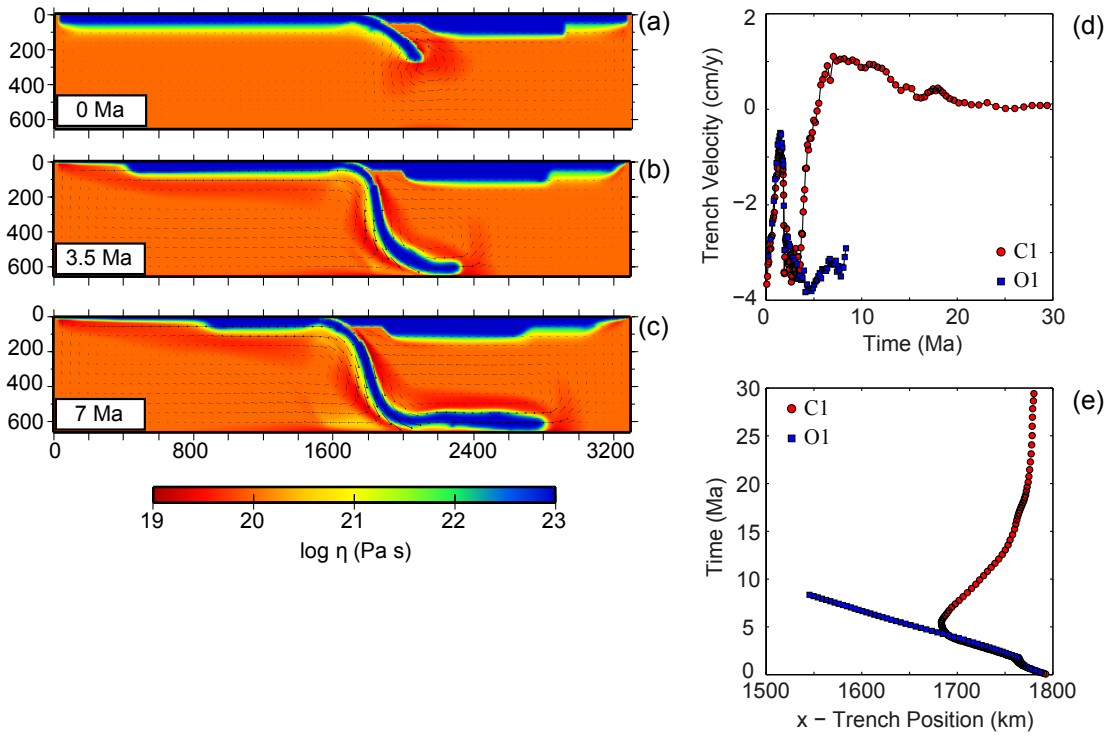

Figure 4.7 - (a-b-c) Viscosity plots of purely oceanic subducting plate model O1; Comparison between model C1 (red dots) and O1 (blue squares): (d) Trench velocity and (e) Trench migration during model evolution.

Continental models with a fixed overriding plate and $\eta_{max}=10^{23}$ Pa s (C5 and C6) show qualitatively the same advancing behaviour when collision occurs (Figure 4.8). The far end of the overriding plate is not free to move, but still, the trench is able to retreat and advance over about 40 km in response to the dynamics of the system. This is due to internal deformation of the overriding plate. This scenario does not occur in the models with a stronger lithosphere with $\eta_{max}=10^{24}$ Pa s (C7 and C8), because the overriding plate is too strong to deform. In that case, the trench is thus almost stationary during every phase of subduction (Figure 4.8b-d).

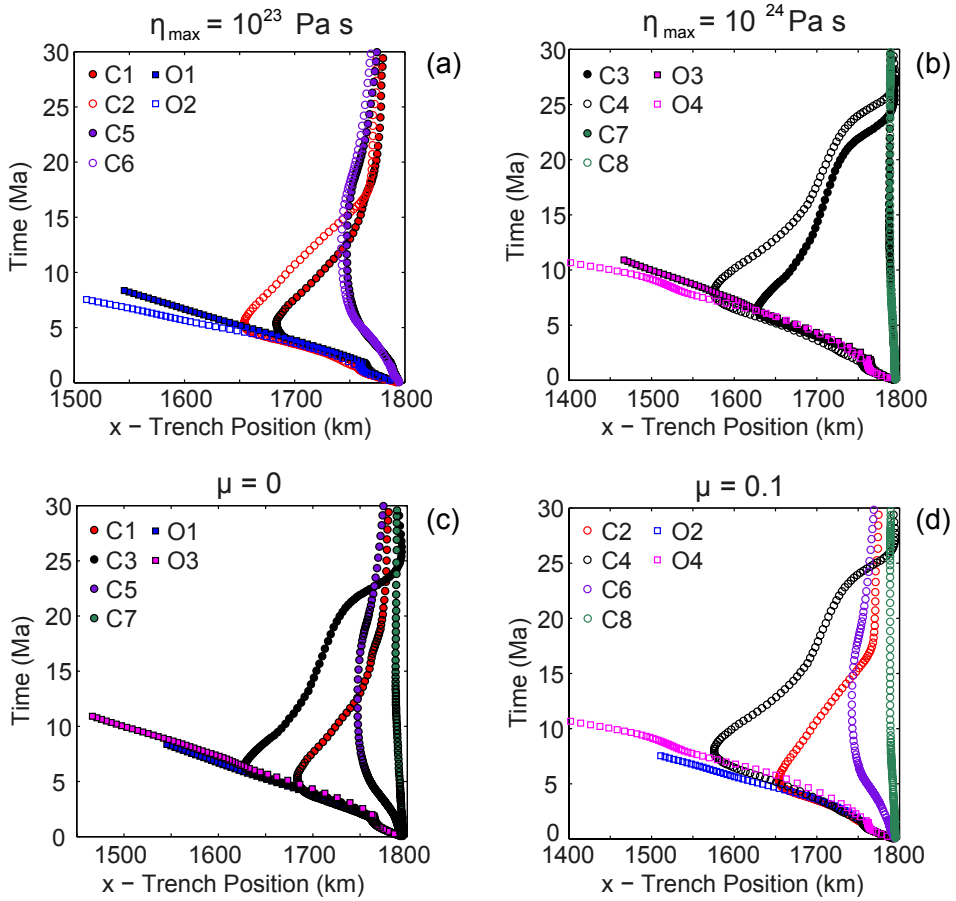

Figure 4.8 - Trench migration for all models with (a) $\eta_{max}=10^{23}$ Pa s, (b) $\eta_{max}=10^{24}$ Pa s, (c) $\mu=0$ and (d) $\mu=0.1$.

4.3.2 Layered Continental Crust

The most common continental rheology model assumes a strong crust and a strong mantle lithosphere separated by a weak ductile layer at the base of the continental crust [*Burov*, 2011; *Handy and Brun*, 2004; *Ranalli*, 1995]. This model, known as "jelly sandwich", appears to be suitable for young continents. The presence of a weak layer within the continental lithosphere is a necessary condition to allow the decoupling between crust and lithospheric mantle, hence, to let delamination occur. However, for cratons, therefore for continents that have a different thermal structure, the lithospheric mantle and the crust are assumed to be coupled [*Burov*, 2011; *Watts*, 2001].

To study which configuration is more suitable for delamination and, on the other hand, which one favours break-off, we performed a set of 42 two-dimensional dynamically self-consistent subduction models where the continental crust is formed by two layers and where we systematically change the viscosity of the lower crust (η_l) and the maximum viscosity of the lithosphere (η_s). We impose a fixed viscosity at the deeper (15-40 km) layer, hence, at the lower crust. This value, η_l, varies from 10^{19} to 10^{21} Pa s and η_s from 10^{22} to 10^{24} Pa s.

Model	Max η slab [Pa s]	η lower crust [Pa s]	Mode
M1	10^{22}	10^{19}	delamination
M2	10^{22}	$5x10^{19}$	delamination
M3	$4x10^{22}$	$2x10^{19}$	delamination
M4	$4x10^{22}$	$4x10^{19}$	delamination
M5	$4x10^{22}$	10^{20}	delamination
M6	$4x10^{22}$	$2x10^{20}$	delamination
M7	$4x10^{22}$	$3x10^{20}$	break-off
M8	$4x10^{22}$	$4x10^{20}$	break-off
M9	$4x10^{22}$	$5x10^{20}$	break-off
M10	$4x10^{22}$	10^{21}	break-off
M11	$5x10^{22}$	$5x10^{19}$	delamination
M12	$8x10^{22}$	10^{20}	delamination
M13	$8x10^{22}$	$2x10^{20}$	delamination
M14	$8x10^{22}$	$3x10^{20}$	delamination
M15	$8x10^{22}$	$4x10^{20}$	break-off
M16	$8x10^{22}$	$5x10^{20}$	break-off
M17	$8x10^{22}$	10^{21}	break-off
M18	10^{23}	$5x10^{19}$	delamination
M19	10^{23}	10^{20}	delamination
M20	10^{23}	$2x10^{20}$	delamination
M21	10^{23}	$3x10^{20}$	delamination
M22	10^{23}	$5x10^{20}$	break-off
M23	10^{23}	10^{21}	break-off
M24	$2x10^{23}$	$2x10^{20}$	delamination
M25	$2x10^{23}$	$4x10^{20}$	delamination
M26	$2x10^{23}$	$5x10^{20}$	break-off
M27	$2x10^{23}$	$8x10^{20}$	break-off
M28	$2x10^{23}$	10^{21}	break-off
M29	$3x10^{23}$	$3x10^{20}$	delamination
M30	$3x10^{23}$	$5x10^{20}$	delamination
M31	$3x10^{23}$	$8x10^{20}$	break-off
M32	$4x10^{23}$	$3x10^{20}$	delamination
M33	$4x10^{23}$	$5x10^{20}$	delamination
M34	$4x10^{23}$	$8x10^{20}$	break-off
M35	$5x10^{23}$	$2x10^{20}$	delamination
M36	$5x10^{23}$	$3x10^{20}$	delamination
M37	$5x10^{23}$	$5x10^{20}$	delamination
M38	$5x10^{23}$	10^{21}	break-off
M39	10^{24}	$5x10^{20}$	delamination
M40	10^{24}	$8x10^{20}$	break-off
M41	10^{24}	10^{21}	break-off

Table 4.2 - Model parameters varied in the different experiments (maximum viscosity of the slab and viscosity of the lower crust) and the resulting mode (4.3.2).

In all set of models of this parametric study we observe two different styles of subduction: (1) delamination (Figure 4.9c) and (2) slight delamination followed by break-off of the slab (Figure 4.9b) (Table 4.2). In both cases the dynamics is similar to the model with a uniform continental crust until collision occurs. At this point, delamination starts: the upper crust separates from the mantle lithosphere, which continues to subduct. In the first style, this separation is sharp and the fully decoupled mantle lithosphere rolls back (Figure 4.9c). Therefore, subduction continues and the delamination front moves away from the suture zone where collision occurred (Figure 4.9f). On the other hand, in the second style, the crust and the mantle lithosphere remain partially coupled. Therefore, the positive buoyancy of the continental crust is still a component of the forces acting on subduction. This is similar to the scenario observed in the uniform continental crust model and, in fact, subduction stops and the oceanic part of the slab detaches from the shallower continental part (Figure 4.9b). Thus, in this style, the delamination front slightly migrates away from the suture zone at the beginning, but, then, it remains stationary (Figure 4.9e).

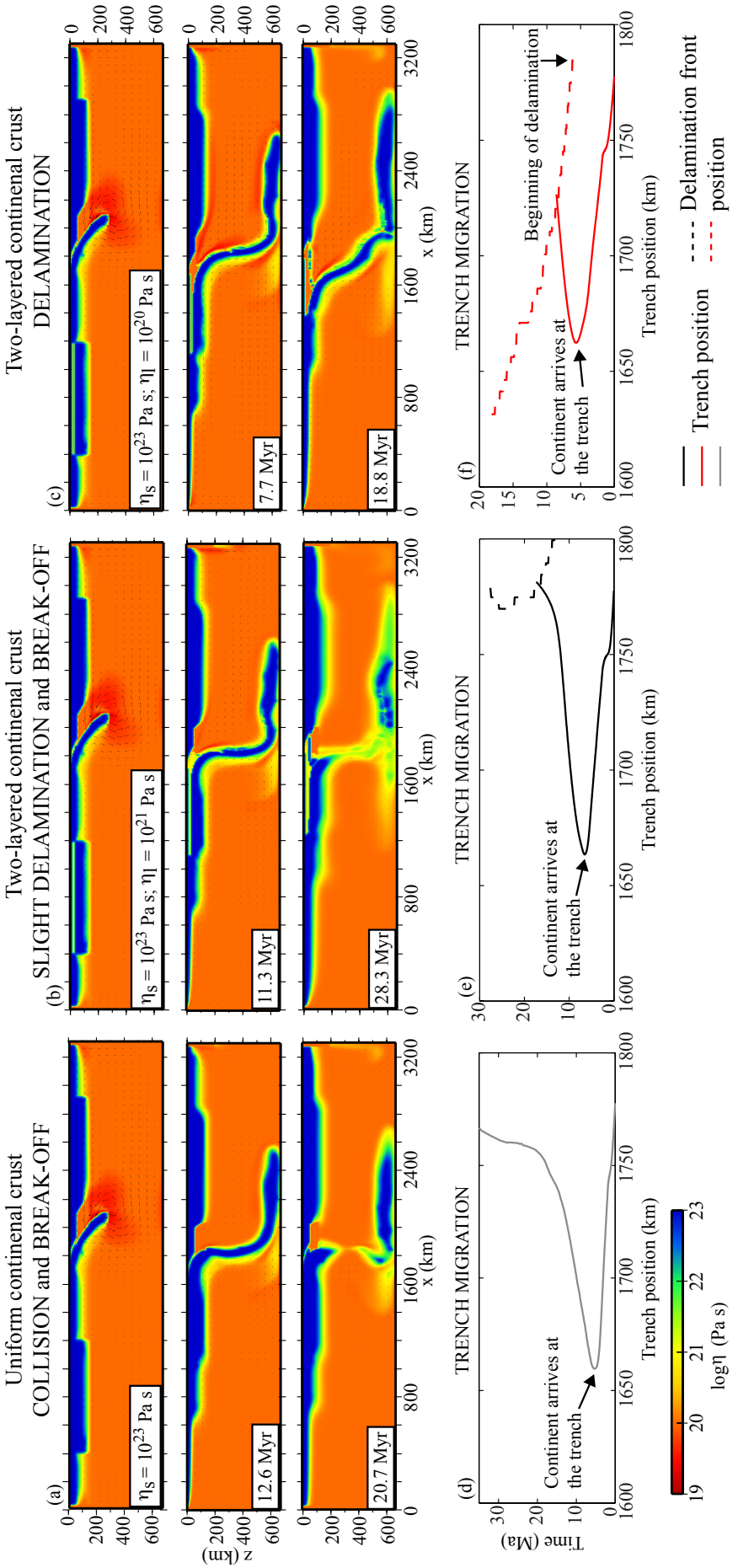
Uniform continenal crust
COLLISION and BREAK-OFF
Two-layered continenal crust
SLIGHT DELAMINATION and BREAK-OFF
Two-layered continenal crust
DELAMINATION
(a)
(b)
(c)
(d)
(e)
(f)
$\eta_S = 10^{23}$ Pa s
$\eta_S = 10^{23}$ Pa s; $\eta_l = 10^{21}$ Pa s
$\eta_S = 10^{23}$ Pa s; $\eta_l = 10^{20}$ Pa s
12.6 Myr
11.3 Myr
7.7 Myr
20.7 Myr
28.3 Myr
18.8 Myr
z (km)
x (km)
TRENCH MIGRATION
Time (Ma)
Trench position (km)
Continent arrives at the trench
Beginning of delamination
Trench position
Delamination front position
logη (Pa s)

Figure 4.9 - The three different resulting scenarios from models with a uniform continental crust (a) and a layered continental crust (b-c): (a) Viscosity plot of model with η_s 1e23 Pa s; (b) viscosity plot of model with η_s 1e23 Pa s and η_l 1e21 Pa s and (c) viscosity plot of model with η_s 1e23 Pa s and η_l 1e20 Pa s. (d-e-f) Trench position during model evolution for the 3 modes: solid lines show trench position; dotted lines indicate the position of the delamination front

All the models, in which η_l and η_s are varied (Table 1), are used to investigate the relationship between these parameters and the subduction style. The results are summarized in Fig. 4.10, where we can observe that low values of η_l favours the delamination style, whereas high values lead to the break-off. In particular, for the studied range of η_s, we find that for $\eta_l \leq 10^{20}$ Pa s delamination always occurs, whereas slab detachment always happens for $\eta_l \geq 8\text{x}10^{20}$ Pa s. For η_l between these two values both scenarios are feasible. We fitted the results of the two-layered crust models to a parameter D that follows a linear scaling law:

$$D = A*\log_{10}(\eta_l) + B*\log_{10}(\eta_s)$$

where the coefficients are: A=0.0718 and B=-0.0208. In this scaling law, D=1 represents the transition between the two styles we observe (solid line in Figure 4.10). In particular, D<1 corresponds to the delamination process, whereas, for D>1 break-off is likely to occur.

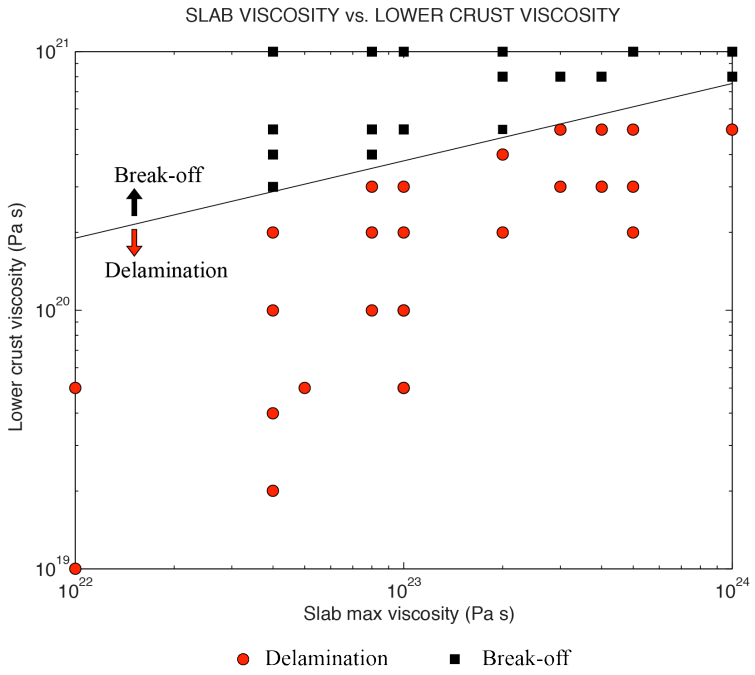

Figure 4.10 - All model results and the calculated scaling law (black line) in a slab viscosity vs. lower crust viscosity plot. Red dots represent delamination mode and black squares represent break-off mode.

4.3.3 Uniform vs. Layered Continental Crust: 3D models

So far I studied the effect of the presence of a continental plateau within the subducting plate on trench migration in a 2D computational domain. The next step is to extend the continental subduction model to the third dimension, in order to study the dynamic response of the whole system to the occurrence of slab detachment or delamination. In particular, the subduction of an oceanic plate that includes a continental plateau in the middle is modelled. In the first model (UCC) the continental crust is uniform (as in 4.3) and break-off of part of the slab is expected, whereas in the second model (LCC) the continental crust is layered (as in 4.3.2) and a constant viscosity of 10^{20} Pa s is imposed for the lower crust. In this case, the decoupling between the continental crust and the lithospheric mantle is expected.

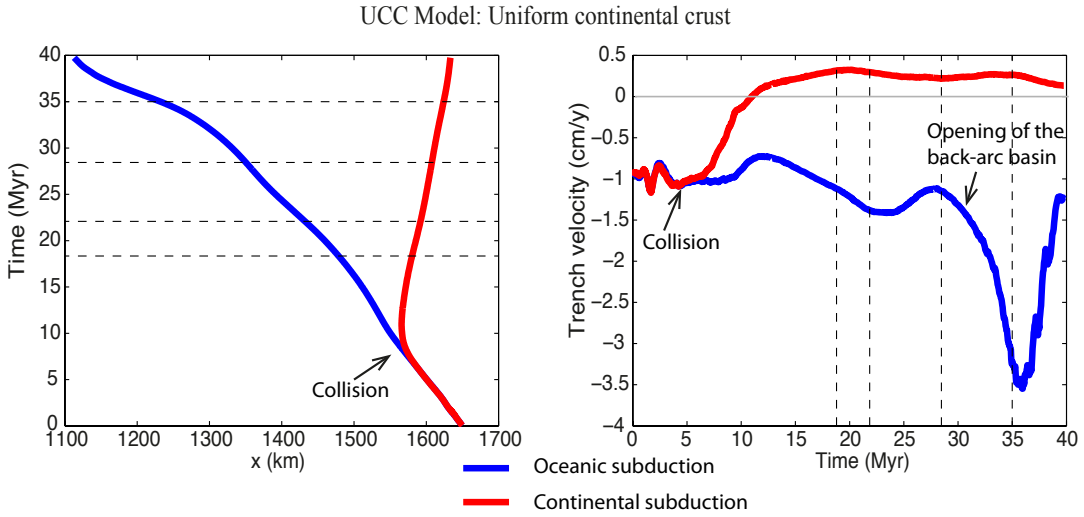

Figure 4.11 - 3D model with a uniform continental crust (UCC): trench migration (left) and velocity (right) during model evolution calculated in two *y*-sections: *y*=660 km (oceanic slab: blue line) and *y* = 1320 (continental slab: red line). Positive velocity corresponds to trench advancing. Dashed lines correspond to panels in Figure 4.12

First, I analyse results of the subduction evolution of model UCC (uniform continental crust). At the early stages of the process only oceanic lithosphere subducts and the whole slab rolls-back with the same velocity along the trench (Figure 4.11). Once the continental plateau arrives at the trench, in that part of the plate the subduction slows down until the trench starts to advance (Figure 4.11). On the contrary, the oceanic sides of the plate keep retreating (Figure 4.11 and Figure 4.12). These different directions of the trench motion cause high deformation of the overriding plate and, therefore, a strong curvature of the trench (Figure 4.13). Also at depth the slab deforms to accommodate the advancing of the middle part of the plate and the retreating of the sides (Figure 4.14).

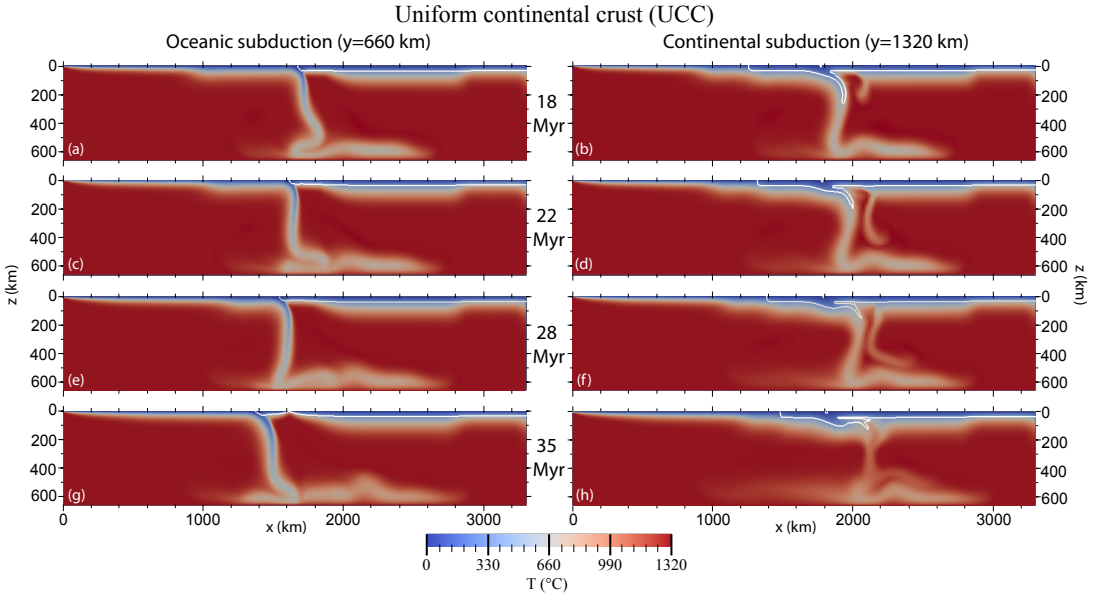

Figure 4.12 - 3D model with a uniform continental crust (UCC): temperature plot of two *y*-sections: *y*=660 km (oceanic subduction: left) and *y* = 1320 (continental subduction: right). The continental crust is outlined by the white line.

The continent subducts to a maximum depth of almost 300 km at ~18 Myr, then the buoyant continental part of the slab starts rising to the surface and the dip angle of the slab decreases (Figure 4.12). This leads to a strong thickening of the continental crust that became double in a 200 km long area (Figure 4.12).

After about 20 Myr from the collision, the overriding plate begins to get weaker where the oceanic slab retreats. This process goes on for few million years, until back-arc basins are formed (Figure 4.12). At this stage the overriding plate does not move anymore as one, but all the deformation is accommodated between the back-arc basin and the trench. This is clear from the horizontal velocities at surface (Figure 4.13) that dramatically increase (from 3.2 cm/y to 6.4 cm/y in about 3 Myr) and, also, looking at the trench velocity in a section at y=660 (in the middle of one of the oceanic sides), where there is a clear peak of fast retreating at about 35 Myr, corresponding to the opening of the back-arc basins (Figure 4.13). The velocity plot of the slab at depth shows that the roll-back of each oceanic side is progressively faster going from the part close to the continent to the edge of the slab (Figure 4.14). At the same time, the break-off of the continental part of the plate is complete both on its front and sides (Figure 4.14). The slab detachment is a further mechanism, in addition to the back-arc basins formation, that favours the fast roll-back of the oceanic sides.

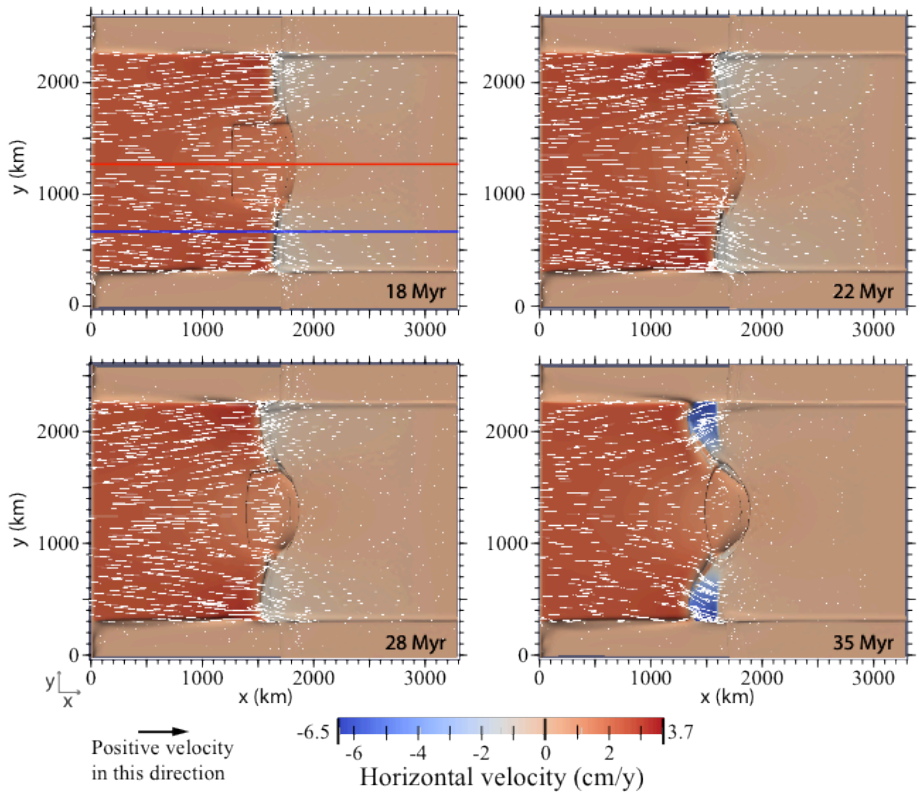

Figure 4.13 - 3D model with a uniform continental crust (UCC): top view. Colours and arrows show the horizontal velocity at the surface (positive velocity is towards the overriding plate). The blue and red lines corresponds to the sections of Figure 4.11 and Figure 4.12.

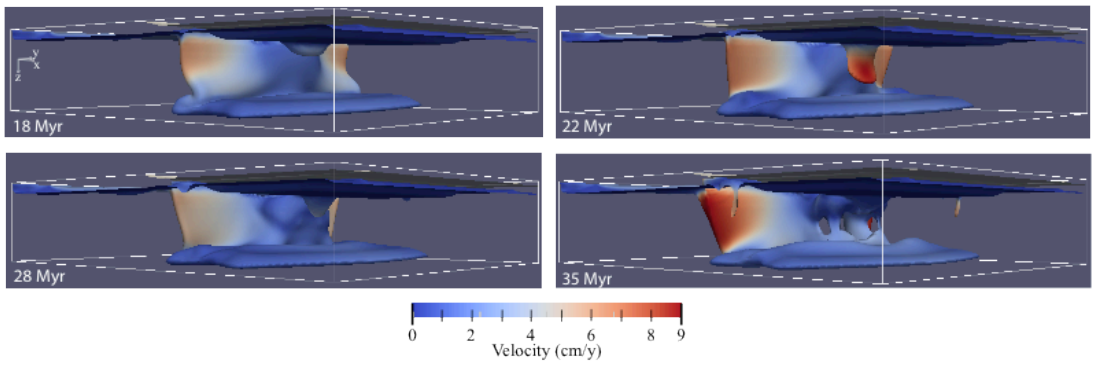

Figure 4.14 - 3D model with a uniform continental crust (UCC): side view of the slab during model evolution. Colours indicate the magnitude of the slab velocity field: the highest velocities are observed at the edges of the oceanic slab while it is retreating (panel 35 Myr).

In the model with a weak lower crust delamination occurs as expected (Figure 4.15). This means that the trench does not advance as observed in the UCC model, but it keeps slowly retreating even after the collision (Figure 4.16). The delamination front moves slightly backwards and let the slab to decrease a little its dip angle. Since the trench retreats in all the parts of the subducting plate (continental and the oceanic sides), no strong trench and slab curvature or large deformation of the overriding plate

are needed. Indeed, the slab and the trench remain fairly straight (Figure 4.17). Moreover, no formation of the back-arc basins in front of the oceanic sides occurs. Finally, the decoupling of the continental crust from the lithospheric mantle leads the continental buoyant material to remain at the surface, unlike in the model UCC (Figure 4.12).

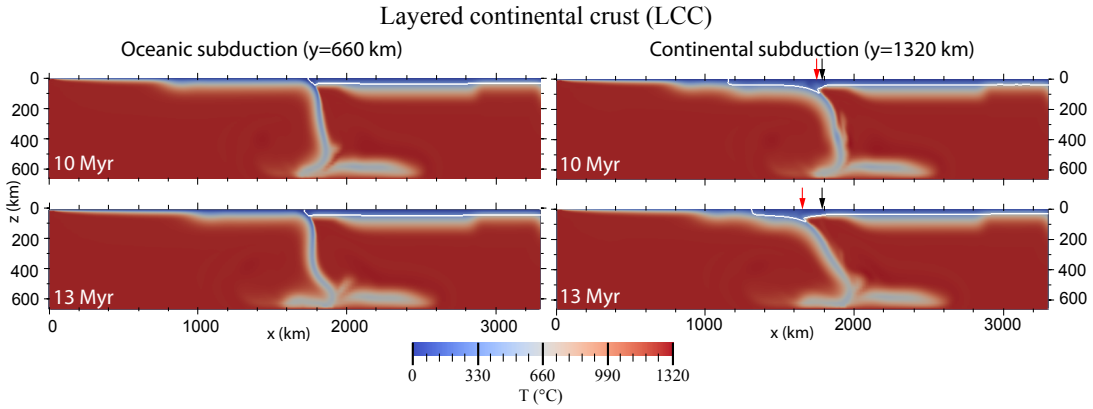

Figure 4.15 - 3D model with a layered continental crust (LCC): temperature plot of two *y*-sections: *y*=660 km (oceanic subduction: left) and *y* = 1320 (continental subduction: right). The continental crust is outlined by the white line. The black arrows indicate the position of the suture zone and the red arrows show the position of the delamination front.

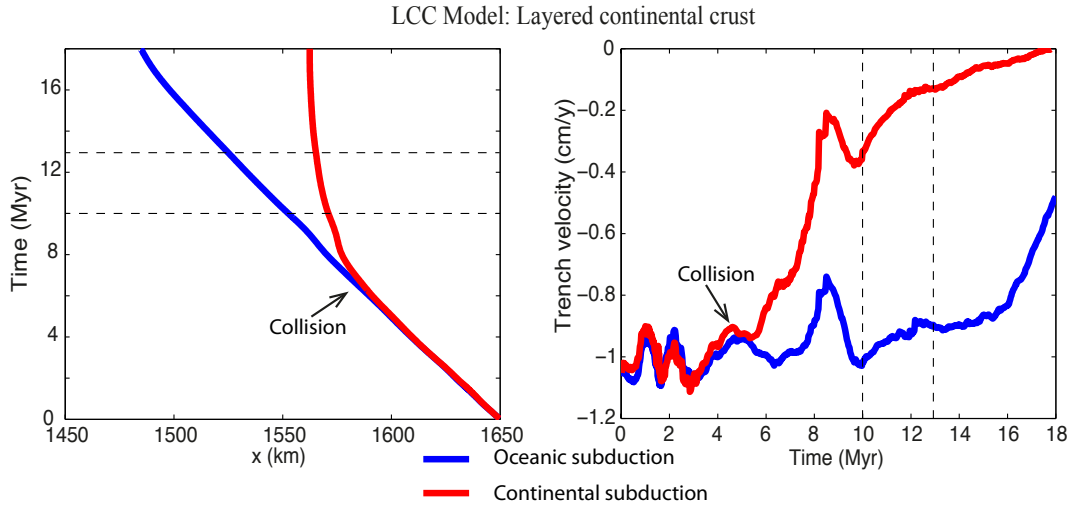

Figure 4.16 - 3D model with a layered continental crust (LCC): trench migration (left) and velocity (right) during model evolution calculated in two *y*-sections: *y*=660 km (oceanic slab: blue line) and *y* = 1320 (continental slab: red line). Dashed lines correspond to panels in Figure 4.15

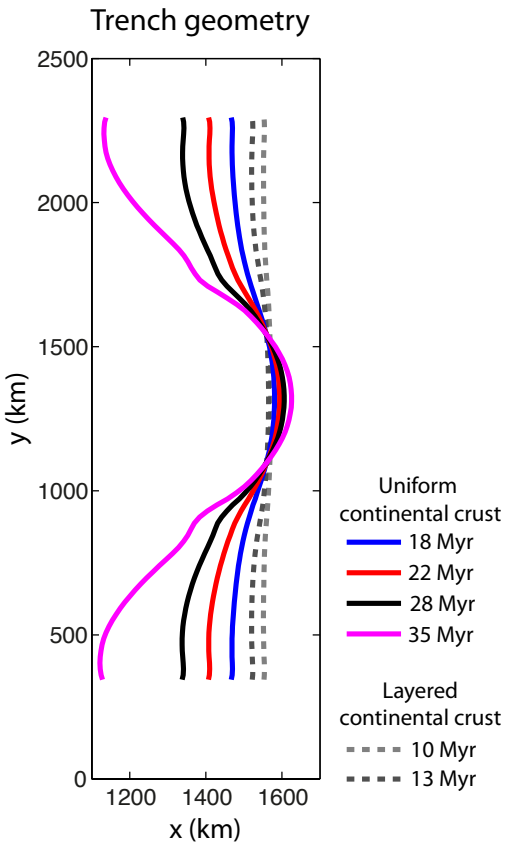

Figure 4.17 - Trench position and shape during the evolution of model with a uniform continental crust (UCC) in solid lines and of the model with a layered continental crust (LCC) in dashed lines.

4.4 Discussion and Concluding Remarks

Our results show that in the models with a uniform continental crust (4.4.1) only the slab detachment occurs (delamination is not possible, since there is no weakness within the crust that allows the decoupling). On the other hand, a setup with a stratified continental crust (4.4.2) can provide different scenarios of continental subduction: the continuation of subduction through the delamination and the end of subduction through the break-off. The models with a uniform continental crust are more suitable for old continental plates, such as cratons, where the crust is coupled with a strong mantle [*Burov*, 2011]. The subduction of an old continent is likely to lead at the slab detachment, as it is proposed for the north African continental margin in the western Mediterranean subduction zone [*Wortel and Spakman*, 2000]. On the contrary, for young continents, the most common rheology model suggests a stratified structure of the lithosphere, where a weak ductile level may lead to a mechanical decoupling between the layers [*Burov*, 2011]. Here, results of models with a uniform and layered continental crust are discussed.

4.4.1 The effect of a continental subducting plate on trench migration

Looking at the whole set of performed model calculations with a uniform continental crust, we observe that, despite different rheological parameters, all models of continental subduction share the same kinematic behaviour (Figure 4.18b): the trench starts to advance once the continent arrives at the subduction zone. Hence, the advancing mode in continental collision scenarios is at least partly driven by an intrinsic feature of the system (Figure 4.19). The locking of the subduction zone on arrival of the continent at the trench induces the deepest part of the slab to move towards the left and the slab to progressively steepen. This, in turn, triggers a small-scale clockwise flow within the mantle behind the slab (Figure 4.19). This flow drives the upper part of the slab towards the overriding plate and results in an advancing trench. This process pursues until the slab reaches a vertical position. The lower the slab angle is before the continental plateau arrives at the trench, the more advancing is needed for the slab to reach its sub-vertical position. Hence, the total amount of advancing depends on the dip of the slab before the collision. E.g., in model C4 the slab is flatter than C1, and therefore the post-collisional trench advance is larger (Figure 4.3 and Figure 4.4).

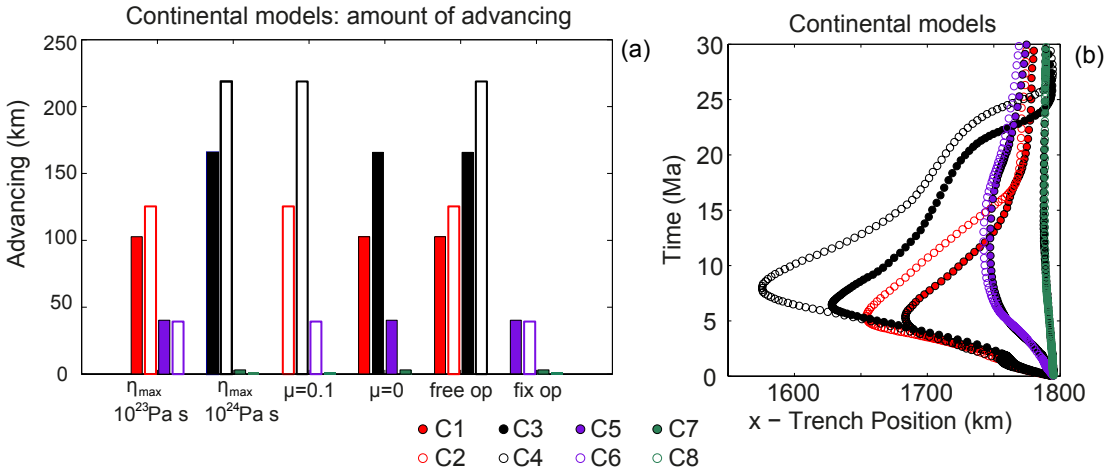

Figure 4.18 - (a) Amount of advancing for all continental models grouped by the changing parameters; free op = free overriding plate, fix op = fixed overriding plate (b) trench migration.

After the vertical position is reached, the advancing velocity decreases. Later, we observe a new peak in the trench velocity plots, related to slab detachment (Figure 4.4b and Figure 4.6b). Over time, the slab weakens thermally, starts stretching, and eventually leads to slab necking and break-off (see *van Hunen and Allen*, 2011, for a more detailed discussion of slab break-off conditions). After the slab detachment, the trench motion stops few million years later. During the stretching of the slab and, eventually, the break-off, the deepest part of the slab is allowed to sink and this activates again the small-scale flow circuit (Figure 4.19). This leads to a new "pulse"

of trench advancing (Figure 4.4b and Figure 4.6b) and an overturning of the slab (Figure 4.19). The resulting geometry of our models during slab detachment resembles to the experimental results of *Regard et al.* [2008] where the return flow during the break-off leads to slab overturning.

Furthermore, during the stretching and subsequent slab break-off, the buoyant, previously subducted, continental material starts rising to the surface (Figure 4.19). This exhumed continental material between the plates pushes them apart, thereby promoting trench migration [*Brun and Faccenna*, 2008]. The weaker the lithosphere is, the more the exhumation is accommodated by internal plate deformation, whereas, for stronger lithosphere the exhumation leads to a larger migration of the plates. Indeed, the increase of velocity in trench motion is more evident in model C4 (Figure 4.18).

Models with the friction coefficient μ=0.1, i.e. a depth-dependent yield strength, show a larger amount of both retreating and advancing (Figure 4.18a) than the ones with a constant (high) yield strength, because of the greater capability of the lithosphere to deform near the weak surface. Moreover, models with a fixed overriding plate and $\eta_{max}=10^{24}$ Pa s show no trench motion because the strength of the lithosphere is too high to deform it. Since internal lithospheric deformation is common in collisional settings (as expressed in e.g. back-arc basins and orogeny), this suggests that the effective viscosity of Earth's lithosphere is less than 10^{24} Pa s.

Although our simplified numerical models are not intended to reproduce the detailed behaviour of any particular subduction zone, obtained results are able to highlight some key features of continental collision. In natural cases, evidences of trench advancing have been recognized in continental collision zones as India-Eurasia and Arabia-Eurasia [*Hatzfeld and Molnar*, 2010; *Replumaz et al.*, 2010]. The values of advancing we obtain in our model (50-220 km; Figure 4.18) are consistent with the amount of trench migration recorded in the Arabia-Eurasia system (50-150 km; [*Hatzfeld and Molnar*, 2010]. On the other hand, our kinematic results cannot explain all of the advancing motion in the India-Eurasia collision (more than 1000 km in 50 Ma) [*Guillot et al.*, 2003; *Matte et al.*, 1997; *Replumaz et al.*, 2010]. Hence it is likely that external forces play a role, such as the pull of neighbouring slabs [*Li et al.*, 2008], or the drag exerted on the base of the lithosphere by a large-scale, convective "conveyor mantle belt" [*Becker and Faccenna*, 2011; *Cande and Stegman*, 2011].

Trench advancing has been observed also in the Melanesian arc system where the Ontong Java plateau, the largest igneous province on Earth, collided with the arc between 25 Ma [*Hall*, 2002; *Knesel et al.*, 2008] and 10 Ma [*Mann and Taira*, 2004]. Buoyancy analyses [*Cloos*, 1993] show that oceanic plateaus with abnormally thick basaltic crust resist subduction and can cause collisional orogenesis. Many authors proposed that after the collision, the anomalously thick lithosphere of the Ontong Java Plateau jammed the trench that led to the break-off of the Pacific plate [*Hall and Spakman*, 2002] and ultimately to a reversal of subduction polarity [*Knesel et al.*, 2008; *Petterson et al.*, 1997].

Our results are also consistent with *Bellahsen et al.* [2003], who observed trench advancing after collision in analogue subduction models. In their models the maximum depth reached by continental material is larger than 360 km, whereas in our study the continent arrives at a maximum of 200 km of depth. This difference is mostly related to a different density contrast (lower in their models) between the continental crust and the mantle material. The key control given by the amount of positive buoyancy of the continent appears evident also when comparing our results with models of *Capitanio et al.* [2010]. They do not obtain trench advancing in only slab-pull-driven subduction models, whereas they observe it only by adding the push of a ridge. Unlike our models, they use a continental lithosphere denser than the underlying mantle. Other analogue [*Faccenna et al.*, 2006; *Regard et al.*, 2005] and numerical models [*De Franco et al.*, 2008; *Duretz et al.*, 2011] studied continental collision, but they cannot be directly compared with our models because they imposed external kinematical constrains by pushing the subducting plate or both plates with a constant velocity or because they assumed a fixed trench [*Gerya et al.*, 2004; *van Hunen and Allen*, 2011].

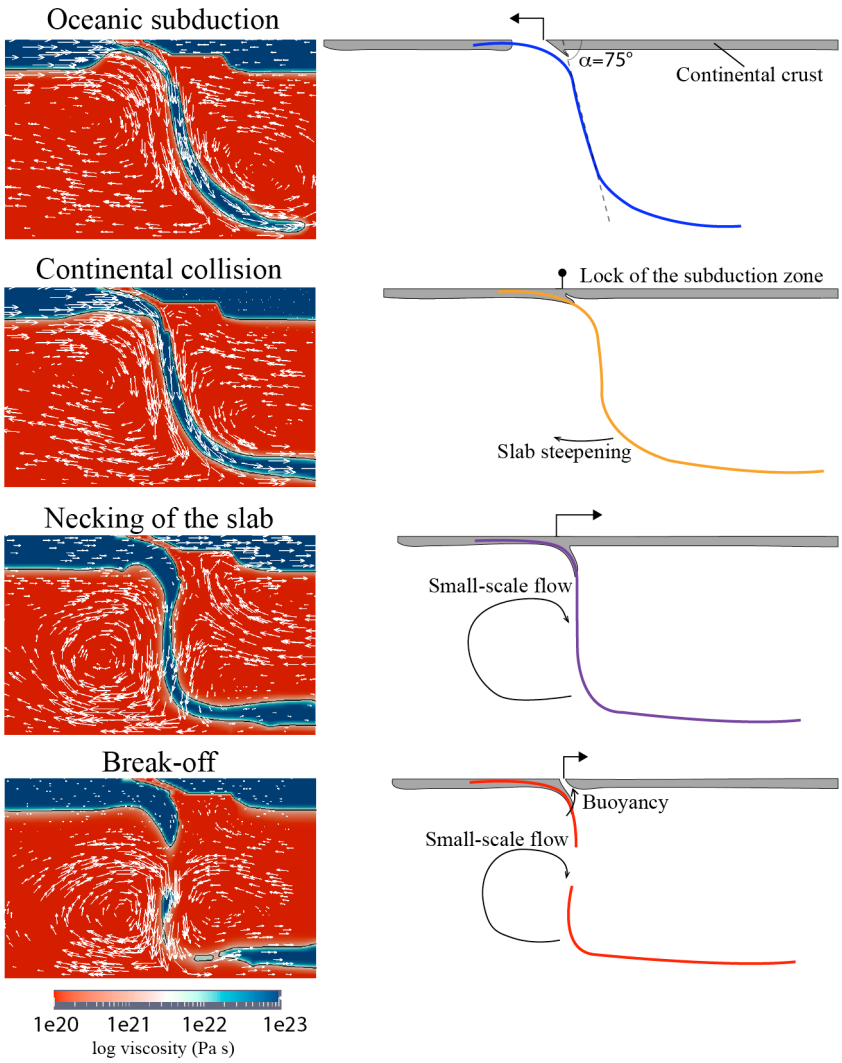

Figure 4.19 - Schematic slab shapes for the continental models C1. The first row shows the shape of the slabs before the continent arrives at the trench and its dip angle. The second row shows all the model evolutions. Third and fourth row show respectively the slab shapes when the necking of the slab starts and when the break-off occurs.

4.4.2 Feasibility of Break-off vs. Delamination

The results of models with a stratified crust show that by changing the viscosity of the lower crust and the maximum viscosity of the lithosphere, both delamination and slab detachment are possible. In particular, delamination is favoured by a low viscosity value of the lower crust, because this makes the mechanical decoupling easier between the crust and the lithospheric mantle. Moreover, our results show that the higher the slab viscosity is, the higher the viscosity of the lower crust is needed to have break-off rather than delamination (Figure 4.10). This is true, for the studied range of η_s, until η_l arrives at a value of 8×10^{20} Pa s. When the viscosity of the lower

crust is larger than this value the decoupling is no longer possible and slab detachment always occurs.

A big difference between the scenarios that we observe lies on the trench migration. In the case of delamination, the continuation of subduction leads to a roll-back of the slab, hence, the delamination front moves away from the suture zone. Between these two spots the lithosphere is very thin, since only the upper crust remains, while the lithospheric mantle subducts. This has been observed, for instance, in the Central Apennines, where delamination of the Adriatic plate occurred [*Channell and Mareschal*, 1989]: seismic profile [*Cassinis et al.*, 2003; *Nicholich and Dal Piaz*, 1992] and analysis of Bouguer gravity anomalies [*Bigi et al.*, 1992; *Scarascia et al.*, 1998] showed that the Moho depth is 38-50 km [*Cassinis et al.*, 2003; *Di Luzio et al.*, 2009], suggesting the absence of the lithospheric mantle. On the other hand, in models with slab detachment, the delamination front cannot migrate much, since the lithospheric mantle is coupled with the buoyant continental crust.

4.4.3 Break-off vs. Delamination: the response of a 3D system

The numerical results of the 3D models show that the rheology of the continental crust has a very strong effect on the dynamics of the whole system, since it influences not only the continental part of plate but also the oceanic sides. As discussed in the previous paragraphs, a weak lower crust enable the decoupling of the buoyant crust from the lithospheric mantle and, therefore, subduction continues, whereas the subduction of a uniform continental crust leads to slab detachment. Indeed, also in a 3D domain, after continental collision, the advancing of the trench and, then, the break-off occur in the model with a uniform continental crust. On the contrary, trench retreating and delamination characterize the model with a layered continental crust.

These two completely different behaviours lead to two distinctive evolutions of the subduction process. For instance, in the UCC model, a strong deformation of the overriding plate is observed both where continental and oceanic subduction occurs. In the first case, the collision brings to a large shortening of the upper plate and, therefore, this part is characterized by a compressive regime. This is similar, for example, to the indentation of India into Eurasia, where the strong shortening leads to the formation of the Himalayan orogeny. Another analogy with the India-Eurasia collisional system is the crustal thickness. Indeed, underneath the Himalaya orogeny the estimated crustal thickness is 80-60 km [*Hatzfeld and Molnar*, 2010]. This is consistent with our results that show a great thickening of the crust when the indentation process is at an advanced stage (Figure 4.12). The similar model in 2D (C1, see 4.3) does not show this feature and, indeed, when the continental slab starts stretching and, eventually, breaks, the buoyant continental material manages to rise at the surface easily, pushing the plates apart. An important difference between models C1 and UCC is the presence laterally of the oceanic lithosphere in the 3D domain that

subducts even after collision in the central part of the plates occurred. The subduction of the oceanic sides provides enough force to move the whole subducting plate, even its continental part, which is pushed towards the upper plate with a velocity much larger than in the 2D model (where the collision leads to a dramatically decreasing of the plate velocities). Thus, in the 3D model, during the stretching and break-off phases, the buoyant material that tries to rise at the surface cannot pushes the plates apart, as in the 2D model, because of the large velocity of the subducting plate. However, it can rise at shallow depths underneath the overriding plate, producing a large area (about 200 km long) of thick continental crust.

Moreover, in UCC the retreating of the oceanic sides causes an extensional regime and the formation of the back-arc basins is an expression of this. Furthermore, also at depth, the high stresses, due to the co-existence of the advancing and retreating mode, lead to a tear of the slab and, eventually, to a lateral break-off.

All these features are not observed in the model where delamination occurs. In fact, the velocities of subduction of the lithospheric mantle and trench retreating in the continental part of the plate are similar to those of the oceanic sides. Thus, the overriding plate does not need to deform and the trench remains fairly straight (Figure 4.17).

CHAPTER 5

The Central Mediterranean subduction zone

5.1 INTRODUCTION

In the previous chapters numerical models of subduction with differences in rheology, geometry and composition of the plates have been developed. The understanding of the dynamics of these end-member cases is essential when modelling more complex subduction zone, such as the Central Mediterranean. All the features studied before are included in this region and they interact during the geodynamic evolution. The main characteristics and the tectonic history of the Central Mediterranean subduction zone are briefly described here.

Over the Cenozoic, Africa has been slowly converging toward stable Eurasia at ~1–2 cm/yr on average, on a NNE path until ~40 Ma, then on a northerly path, and finally rotating to a N20°W convergence [*Dewey et al.*, 1989; *Faccenna et al.*, 2007b; *Jolivet and Faccenna*, 2000]. This slow convergence has led to the build up of the Alpine chain in sites where continental collision (i.e., Adria - Eurasia) has taken place. At ~30–20 Ma, the already slow convergence decreased [*Jolivet and Faccenna*, 2000; *Silver et al.*, 1998]. Although the precise paleogeographic configuration is still debated, a general agreement exists about the presence of a small Mesozoic oceanic domain between Africa and Eurasia that has facilitated, from 30 Ma onward, the retreat of the trench and the opening of the back-arc basins [*Le Pichon*, 1982; *Malinverno and Ryan*, 1986]. The Calabrian slab rolled back for more than 800 km since subduction started with an episodic behaviour and peaks of trench motion velocity of ~6 cm/yr [*Faccenna et al.*, 2001; *Faccenna et al.*, 2007b] (Figure 5.1). Its rapid and large retreating is the cause of the arc-shaped Calabrian trench that we observe in the present-day configuration.

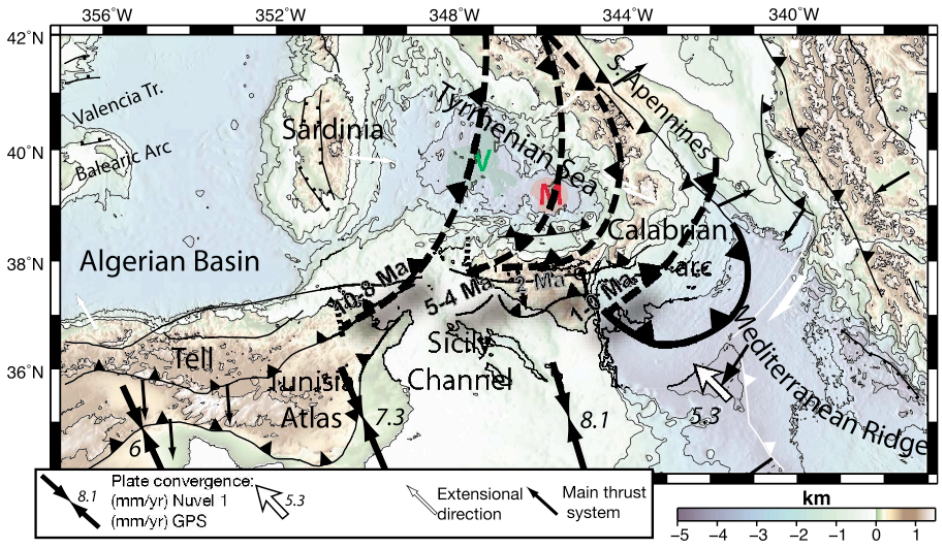

Figure 5.1 - Schematic tectonic evolution of the central Mediterranean region over the past 10 Myr (from [*Faccenna et al.*, 2011]). The trace of the Wadati- Benioff zone at 50 km depth is marked with thick curves. Triangles indicate the sense of subduction. Note the progressive lateral disruption of the subduction zone during the back arc extensional phases. At circa 1 Ma, the system reorganized and a new compressional front developed in the southern Tyrrhenian region (north of Sicily). V indicates the Vavilov basin and M indicates the Marsili basin.

The first episode of the back-arc extensional process led to the opening of the Liguro-Provençal Basin. The age of the synrift and postrift deposits [*Burrus*, 1984; *Cherchi and Montadert*, 1982; *Séranne*, 1999] indicates that the initial phase of stretching lasted from 30 to 21 Ma before lithospheric break-up and oceanic spreading occurred (21–16 Ma), while the Sardinia-Corsica block rotated counterclockwise [*Speranza*, 1999; *Van der Voo*, 1993]. The rifting episode in the Tyrrhenian sea probably started ~12–10 Ma and was followed by pulses of oceanic spreading that migrated eastward from the Vavilov basin to the Marsili basin [*Guillaume et al.*, 2010]. The opening of the basins has been related to the thinning of the oceanic slab and to the formation of slab windows both in the African part of the subducting plate and the Adriatic one [*Faccenna et al.*, 2001; *Faccenna et al.*, 2007b; *Guillaume et al.*, 2010]. In fact, *Faccenna et al.* [2007] propose that the back-arc extension process is controlled by the geometry of the deforming subducting lithosphere. In other words, they suggest that the lateral tear and separation of the Ionian slab from the contiguous buoyant continental domains permit its retrograde motion and, in turn, produce back-arc extension.

A snapshot of the present-day configuration of the Central Mediterranean subduction zone is provided by tomographic images (Figure 5.2). Many seismic analyses showed the presence of a high-velocity anomaly beneath the Calabrian arc that corresponds to the cold subducted Ionian slab [*Piromallo and Morelli*, 2003]. This is also well recorded by the seismicity, which is distributed along a narrow (~200 km) and steep (~70°) Wadati-Benioff plane, which strikes SW-NE and dips NW,

down to ~500 km [e.g., *Anderson and Jackson*, 1987; *Giardini and Velonà*, 1991; *Selvaggi and Chiarabba*, 1995].

The abundance of geological data, geophysical analyses and studies on the Central Mediterranean subduction zone makes it an ideal case of study to investigate how the main geodynamics features interact during the evolution of the system. The aim of this work is to study the evolution of subduction over the last 40 Myr in the Central Mediterranean and to unravel how this is related with the main tectonic features recognized in this region. This is the first part of a more extended study on the dynamics of the Mediterranean over the last 80 Myr, which aims at investigating the interaction between different chains (Alps-Apennines and Alps-Carpathian) and their peculiar arc-shape edges.

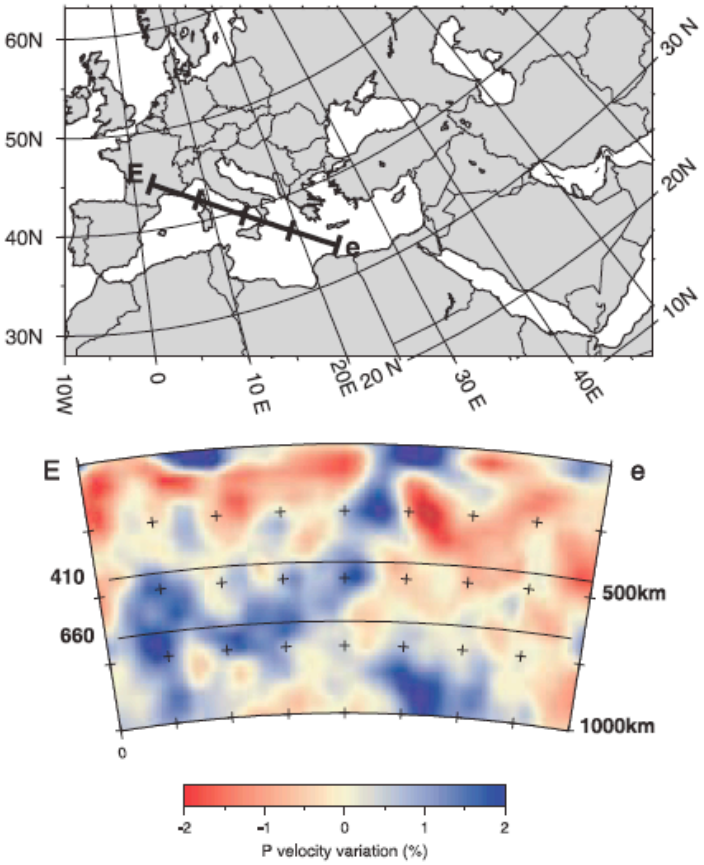

Figure 5.2 - Tomographic image of a NW-SE section. The top map illustrates the section location. The tomographic image shows a high velocity anomaly on the Ionian side of the Calabrian Arc connected to the fast structure steeply dipping below the arc into the mantle and bending horizontally in the transition zone (from *Piromallo and Morelli*, 2003)

5.2 MODEL SETUP

The evolution of the Central Mediterranean subduction is reproduced in a 3D computational domain 660 km deep and with an aspect ratio of 1:5:4. The initial

geometry of the subducting plate corresponds to the paleogeography of about 40 Myr ago proposed in the geodynamic reconstructions of this area [*Brun and Faccenna*, 2008; *Jolivet et al.*, 2008; *Vignaroli et al.*, 2008] (Figure 5.3). The narrow oceanic part of the subducting plate corresponds to the Calabrian plate. The two continental sides correspond to the Adria and Africa plate and the overriding plate corresponds to Eurasia. The first part of the subducting plate (300 km) is set to be oceanic along the whole plate to provide enough slab pull before collision occurs, and mimics the pre-collisional closure of the Neo-Tethys ocean. The model geometry is simplified compared to the paleogeographic reconstructions, since the aim of this work is not to replicate the Central Mediterranean dynamics in detail, but to study the first order effect of the main features within the system.

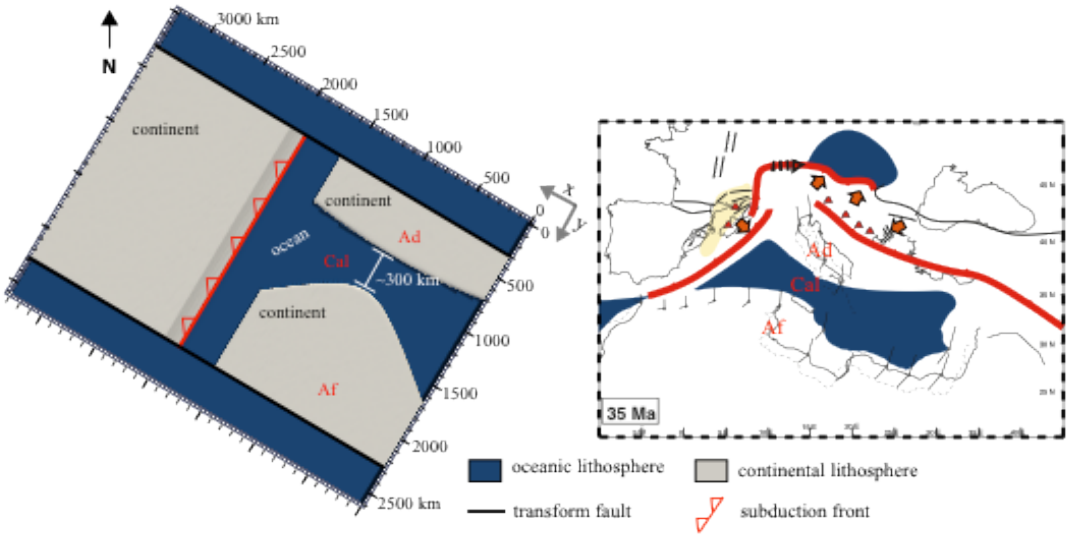

Figure 5.3 - Top view of the initial model geometry (on the left) compared with a geodynamic reconstruction of the Central Mediterranean at 35 Ma (courtesy of C. Faccenna) (on the right). The blue areas indicate the oceanic part of the plates: the first part of the subducting plate (~300 km) is set to be oceanic to simulate the closure of the Neo-Tethys ocean. The other oceanic part of the plate corresponds to the Calabrian slab that is surrounded by continental lithosphere (grey), representing the African plate at south and the Adria plate at north. The red line indicates the subduction front, the black line show the presence of the transform faults.

The initial temperature field for the oceanic lithosphere is calculated following the half-space cooling solution for a 80-Myr old plate [*Turcotte and Schubert*, 2002]. The resulting thermal structure is similar to the one expected also for older plates [*Ritzwoller et al.*, 2004]. For the continental lithosphere, temperature extends linearly from 0° C at the surface to the mantle reference temperature at 150 km depth. A 40-km deep continental crust is characterized by positive buoyancy (the density difference between the continental crust and the mantle material is 600 kg/m^3), which creates a resisting force to subduction when the continental block inside the subducting plate arrives at the trench.

The initiation of subduction is not studied here, since this model starts with already ~300 km of subducted lithosphere. The time zero of the model, thus, corresponds roughly at 40 Ma in the tectonic history, when the last wide part of the Mesozoic ocean is consuming.

The top boundary has a fixed temperature of 0°C, at the *y*-boundaries dT/dx=0, whereas all the other boundaries have a fixed mantle temperature T_m=1350°C. Velocity boundary conditions are free-slip on all but the bottom boundary, where a no-slip condition is applied. The presence of weak transform faults at *y*=330 km and *y*=2310 km with the same width and viscosity of the subduction fault enable the motion of the plates. The overriding plate is fixed at the right hand side, while the subducting plate is free to move. A maximum viscosity value is set to 10^{23} Pa s. The friction coefficient is assumed to be μ=0.1, the yield stress at surface is τ_0=40 MPa and the maximum yield stress is τ_{max}=400 MPa (see 2.5).

5.3 RESULTS

At the early stage of the model calculation, the oceanic slab rolls back with the same velocity along the whole plate (Figure 5.4). Then, after about 8 Myr from the beginning of the model, both continental blocks arrive at the trench causing lateral variations of subduction and trench velocities. The first clear effect of these lateral variations is the curvature of the trench: the oceanic part of the slab is rolling back, whereas the continental sides resist to subduction, starting a strong decrease in the subduction velocities (Figure 5.5). Trench velocities calculated at two sections in the middle of the continental blocks are always slightly above zero since the continent enters the subduction zone and, therefore, the trench slowly advances (Figure 5.4). On the contrary, the subduction of the oceanic slab continues and the trench keeps retreating (Figure 5.6). After about 12 Myr from the occurrence of collision, a back-arc basin in front of the oceanic slab starts to form (Figure 5.7). This leads to a sudden increase of the retreating velocity with maximum value of horizontal velocities within the basin of ~4 cm/y (Figure 5.5).

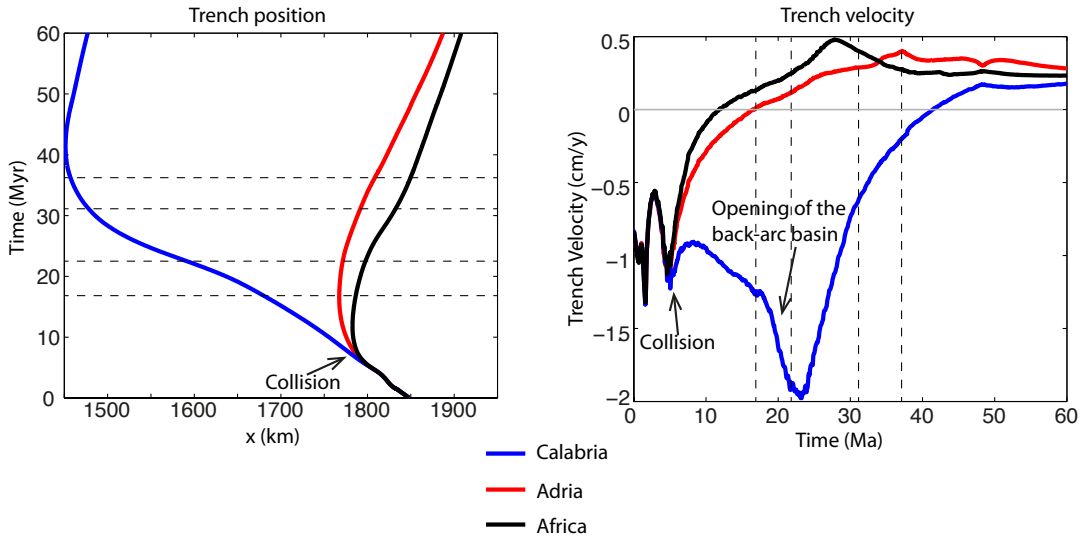

Figure 5.4 - Trench migration (left) and velocity (right) during model evolution calculated in three *y*-sections in the middle of each part of the subducting plate: Adria (red line), Calabria (blue line) and Africa (black line). Positive velocity corresponds to trench advancing. Dashed lines correspond to panels in Figure 5.5 and Figure 5.6

Looking at the curved shape of the slab it appears evident that the oceanic subduction drags part of the continental slabs (Figure 5.5). This force pulls down also the buoyant continental material that reaches a maximum depth of ~400 km in the Adria plate and ~300 km in the Africa plate (Figure 5.5). Moreover the Adriatic slab is deformed and rotated by the drag of the oceanic slab and by the flow of the mantle. At this stage, the continental slabs are getting weaker due to the opposing forces that act on them: the resisting force to subduction provided by the buoyant continental crust and the pull of the deep oceanic slab. This leads to a necking process, which goes on until slab break-off occurs (Figure 5.5). For the African slab this happens after about 22 Myr from the collision: the break starts at its centre and it propagates laterally. The slab detachment of the Adria plate occurs ~5 Myr later.

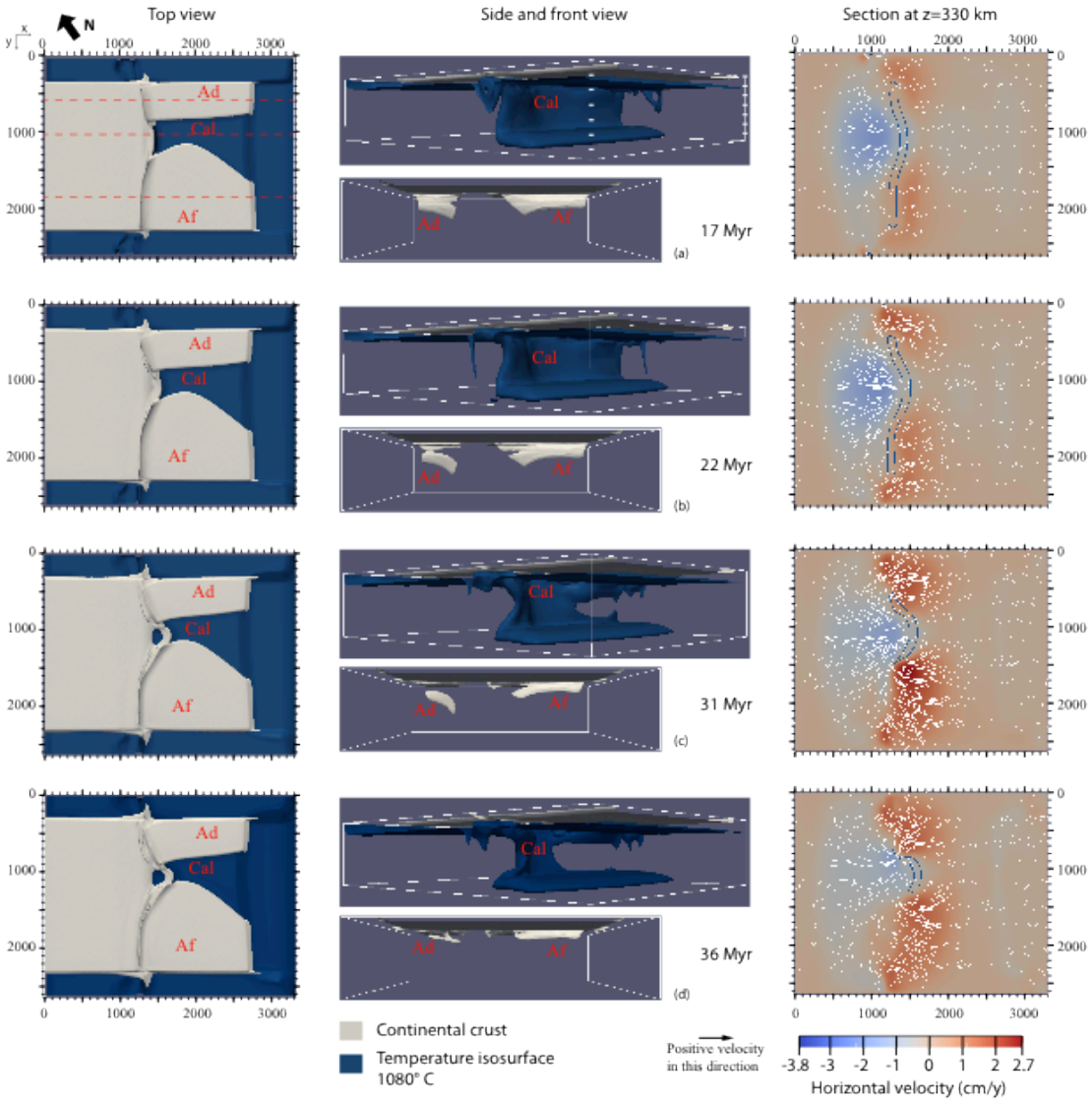

Figure 5.5 - Model evolution - for each time (a,b,c,d) 4 plots are shown: a top view of the model geometry at the surface (left column), a side view of the slab shape (temperature isosurface of 1080° C) (middle top), a front view of the position of the buoyant continental crust (middle bottom) and the horizontal velocity in a *z*-section at z=330 km. In this last plot, colours and arrows indicate the velocity field (positive velocity towards the overriding plate) and the slab is outlined by the blue line.

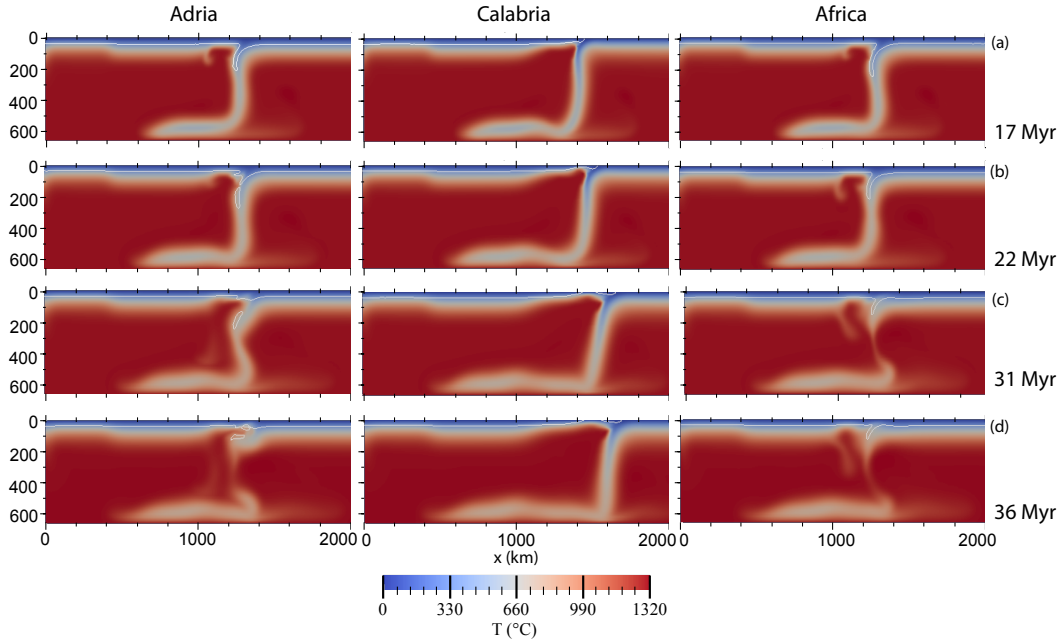

Figure 2.6 - Model evolution: temperature plot in the three *y*-sections in the middle of each part of the subducting plate: Adria (left column), Calabria (middle column) and Africa (right column). The continental crust is outlined by the white line.

The break-off of the slab has two main effects. The first one is related to the mantle flow: a large amount of mantle material flows through the slab window formed by the break-off. Velocities of about 3 cm/y are observed in a horizontal section at z=300 km (Figure 2.5). The second effect is the rising of the continental material that was brought at depth by the pull of the oceanic slab. Indeed, in a very short time (~5 Myr) it arrives at shallow depths (Figure 2.5c-d). In the last stage of the model, the slab is formed only by its oceanic part that gets progressively thinner.

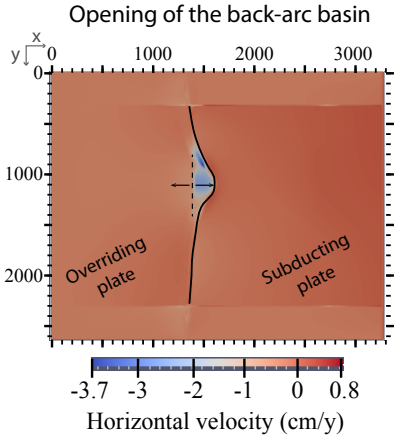

Figure 2.7 - Top view of the horizontal velocity at the surface. Negative velocity (blue) is towards the subducting plate. Velocities are almost zero in the whole surface except in front of Calabria, where velocities of almost 4 cm/y are observed. These velocities are the consequence of the fast retreating of the oceanic slab and the opening of the back-arc basin (outlined by the arrows). The solid black line indicates the trench position and shape.

5.4 Discussion and Preliminary Remarks

The complex tectonic history of the Central Mediterranean is caused by the large rheological, geometrical and compositional variations within a relative small system. Moreover episodic trench migration and large differences in the subduction velocities characterize this area, making a tectonic reconstruction difficult. The numerical model results allow us to relate the main tectonic episodes of the Central Mediterranean with the evolution of the subduction process.

At about 35 Ma the collision of Adria with Eurasia occurs [*Faccenna et al.*, 2001; *Jolivet et al.*, 2008; *Vignaroli et al.*, 2008]. At this stage the trench starts to migrate with different velocities. Indeed, the Calabrian slab rolls back, whereas the continental slab slows down. This causes a rotation of the Adria plate and a strong curvature of the trench.

The formation of the Liguro-Provençal back-arc basin at ~30-16 Ma is interpreted as a consequence of the interaction of the slab with the upper-lower mantle discontinuity [*Faccenna et al.*, 2001]. Afterward, a new episode of extension opens the Tyrrhenian basin (starting at ~12-10 Ma). In our model, only one back-arc basin is formed. This might be caused by the fact that when the slab arrives at the 660 km discontinuity, collision is not occurred yet and, therefore, there are no large differences in trench velocities along the plate. Moreover, the assumption of a closed and impermeable upper-lower mantle discontinuity in the model might have an effect on the way the slab interacts with it. However, our model is able to simulate the formation of a back-arc basin due to the fast retreating of the oceanic part of the slab that forces the overriding plate to deform and weakens until a rift is created. Maximum opening velocities during this phase in the model (~4 cm/y) are smaller than those estimated during the opening of the Tyrrhenian (~7-19 cm/y [*Guillaume et al.*, 2010]). The maximum amount of retreating of the Calabrian slab obtained in our model is about 400 km, which is less then the estimated value from geodynamics reconstruction (800 km in 80 Myr). These differences might be due to the fact that our model does not include the possibility to create a transform fault at the surface and therefore it cannot model the formation of a dextral transform boundary zone in the Sicily channel. The presence of this transform fault enables the Calabrian slab to move more freely, thus, to increase the amount of retreating.

The opening of the Tyrrhenian basin is roughly contemporaneous with the detachment of the African slab (~10 Ma) and the rapid propagation of the break-off laterally [*Carminati et al.*, 1998; *Faccenna et al.*, 2007b; *Jolivet et al.*, 2008; *Wortel and Spakman*, 2000]. The newly formed slab window allows the mantle material to flow from behind the slab around its edge. Evidence for such mantle flow is recorded in the geochemical signatures of the magmatism in the Tyrrhenian [e.g., *Beccaluva et al.*, 1998; *Faccenna et al.*, 2007b; *Gasperini et al.*, 2002]. The break-off of the Adriatic plate occurs about 5 Myr later after it has been strongly deformed and rotated

by the mantle flow and the dragging forces of the Calabrian slab. These results are in good agreement with the reconstruction of *Faccenna et al.* [2007]. They suggested that the narrow and rapidly retreating Calabrian slab results from the lateral disruption of the western Mediterranean subduction zone produced by the formation of two large slab windows, in the southern Tyrrhenian Sea and in the southern Apennines. Moreover, they speculate that the Calabrian slab has been progressively eroded by means of mechanical and thermal processes. Indeed, in the last stages of the presented numerical model the Calabrian slab is narrower and narrower and it is completely detached from the rest of the subducting plate, except at depth. This is also in agreement with tomographic images of this region that shows a narrow high velocity area underneath Calabria vertically continuous from the surface to the 660 km discontinuity on which it lies. This has been interpreted as the cold subducted lithosphere [*Piromallo and Morelli*, 2003]. At about 500 km of depth another high-velocity area that spreads all over central Europe and the western Mediterranean is found. This area probably gathers the material from different slabs (i.e. Alpine, Betic-Alboran, Algerian, Apenninic and Calabrian slabs) that subducted during the evolution of the Central Mediterranean [*Wortel and Spakman*, 2000].

These preliminary results form an important first step for the development of a more extended model of the Mediterranean that will include also the Alpine subduction with the aim to study the interaction between these different chains and their peculiar arc-shape edges.

CHAPTER 6

Summary and Conclusions

The trench motion is influenced by the rheological, geometrical and compositional properties of the plates. In nature, these properties vary within the same subduction zone, making difficult the understanding of the subduction dynamics and the tectonic reconstruction. Furthermore, trench migration has important consequences for tectonics such as back-arc spreading, but also for large-scale upper mantle dynamics. In this Thesis, the effect of heterogeneities within the subducting plate on the dynamics of subduction is investigated by using the finite element technique. In particular, I studied the motion of the trench for oceanic and continental subduction, first, separately, and, then, together in the same system to understand how they interact.

The numerical models of purely oceanic subduction showed that trench retreats with different velocities for different plate age and, therefore, for different thickness and strength of the lithosphere. Accordingly to that, a direct consequence of including lateral age variations within the subducting plate in a three-dimensional model is the differentiate trench motion that leads to the deformation of the overriding plate and, thus, to the formation of a curve trench.

The next step was to study the continental subduction and its influence on the geometry and kinematics of the process. Our results showed that despite different rheological parameters, all models of continental subduction with a uniform crust share the same kinematic behaviour: the trench starts to advance once the continent arrives at the subduction zone. Hence, the advancing mode in continental collision scenarios is at least partly driven by an intrinsic feature of the system. Moreover, we found that by changing the viscosity of the lower crust and the maximum viscosity of the lithosphere, both delamination and slab detachment can occur. In particular, delamination is favoured by a low viscosity value of the lower crust, because this makes the mechanical decoupling easier between the crust and the lithospheric mantle. These features are observed both in 2D and 3D models, but the numerical results of the 3D models also showed that the rheology of the continental crust has a very strong effect on the dynamics of the whole system, since it influences not only the continental part of plate but also the oceanic sides.

Finally, a better understanding of the dynamics of trench migration in different scenarios allowed me to study the evolution of subduction over the last 40 Myr in the Central Mediterranean with the aim of unravelling how this is related with the main tectonic features recognized in this region. The numerical model was able to reproduce the main tectonic features present in this area (e.g., the formation of a back-arc basin, the fast retreating of the Calabrian slab and the pronounced trench curvature). These preliminary results form an important first step for the development of a more extended model of the Mediterranean that will include also the Alpine subduction with the aim of investigating the interaction between different chains (Alps-Apennines and Alps-Carpathian) and their peculiar arc-shape edges.

BIBLIOGRAPHY

Anderson, H., and J. Jackson (1987), The deep seismicity of the Tyrrhenian Sea, *Geophysical Journal of the Royal Astronomical Society*, *91*(3), 613-637.

Andrews, E. R., and M. I. Billen (2009), Rheologic controls on the dynamics of slab detachment, *Tectonophysics*, *464*(1-4), 60-69.

Beccaluva, L., F. Siena, M. Coltorti, A. D. Grande, A. L. Giudice, G. Macciotta, R. Tassinari, and C. Vaccaro (1998), Nephelinitic to Tholeiitic Magma Generation in a Transtensional Tectonic Setting: an Integrated Model for the Iblean Volcanism, Sicily, *Journal of Petrology*, *39*(9), 1547-1576.

Becker, T. W., and C. Faccenna (2009), A review of the role of subduction dynamics for regional and global plate motions, in *Subduction Zone Geodynamics*, edited by S. Lallemand and F. Funiciello, pp. 3-34, Springer.

Becker, T. W., and C. Faccenna (2011), Mantle conveyor beneath the Tethyan collisional belt, *Earth Planet Sc Lett*, *310*, 453-461.

Becker, T. W., C. Faccenna, R. J. O'Connell, and D. Giardini (1999), The development of slabs in the upper mantle: Insights from numerical and laboratory experiments, *J. Geophys. Res.*, *104*(B7), 15207-15226.

Bellahsen, N., C. Faccenna, and F. Funiciello (2005), Dynamics of subduction and plate motion in laboratory experiments: Insights into the "plate tectonics" behavior of the Earth, *J Geophys Res-Sol Ea*, *110*(B1).

Bellahsen, N., C. Faccenna, F. Funiciello, J. M. Daniel, and L. Jolivet (2003), Why did Arabia separate from Africa? Insights from 3-D laboratory experiments, *Earth Planet Sc Lett*, *216*(3), 365-381.

Bigi, G., D. Cosentino, M. Parotto, R. Sartori, and P. Scandone (1992), Structural Model of Italy and Gravity Map., *Quaderni de "La Ricerca Scientifica"*, *104*(3), CNR, Progetto Finalizzato Geodinamica, Roma

Billen, M. I. (2008), Modeling the dynamics of subducting slabs, *Annu Rev Earth Pl Sc*, *36*, 325-356.

Billen, M. I., and G. Hirth (2007), Rheologic controls on slab dynamics, *Geochem Geophy Geosy*, *8*.

Bird, P. (1979), Continental delamination and the Colorado Plateau, *Journal of Geophysical Research*, *84*(B13), 7561-7571.

Brun, J. P., and C. Faccenna (2008), Exhumation of high-pressure rocks driven by slab rollback, *Earth Planet Sc Lett*, *272*(1-2), 1-7.

Burov, E. B. (2011), Rheology and strength of the lithosphere, *Mar Petrol Geol*, *28*(8), 1402-1443.

Burrus, J. (1984), Contribution to a geodynamic synthesis of the Provençal Basin (North-Western Mediterranean), *Marine Geology*, *55*(3-4), 247-269.

Byerlee, J. D. (1978), Friction of rocks, *Pure Appl. Geophys.*, *116*, 615-626.

Cande, S. C., and D. R. Stegman (2011), Indian and African plate motions driven by the push force of the Reunion plume head, *Nature*, *475*(7354), 47-52.

Capitanio, F. A., D. R. Stegman, L. N. Moresi, and W. Sharples (2010a), Upper plate controls on deep subduction, trench migrations and deformations at convergent margins, *Tectonophysics*, *483*(1-2), 80-92.

Capitanio, F. A., G. Morra, S. Goes, R. F. Weinberg, and L. Moresi (2010b), India-Asia convergence driven by the subduction of the Greater Indian continent, *Nat Geosci*, *3*(2), 136-139.

Carminati, E., M. J. R. Wortel, W. Spakman, and R. Sabadini (1998), The role of slab detachment processes in the opening of the western-central Mediterranean basins: some geological and geophysical evidence, *Earth Planet Sc Lett*, *160*, 651-655.

Cassinis, R, Scarascia, S, Lozej, and G. A (2003), The deep crustal structure of Italy and surrounding areas from seismic refraction data. A new synthesis, *Bollettino della Società geologica italiana*, *122*(3), 12.

Channell, J. E. T., and J. C. Mareschal (1989), Delamination and asymmetric lithospheric thickening in the development of the Tyrrhenian Rift, *Geological Society, London, Special Publications*, *45*(1), 285-302.

Chapple, W. M., and T. E. Tullis (1977), Evaluation of forces that drive the plates, *J. Geophys. Res.*, *82*(14), 1967-1984.

Chemenda, A. I., M. Mattauer, and A. N. Bokun (1996), Continental subduction and a mechanism for exhumation of high-pressure metamorphic rocks: new modelling and field data from Oman, *Earth Planet Sc Lett*, *143*(1-4), 173-182.

Chemenda, A. I., J. P. Burg, and M. Mattauer (2000), Evolutionary model of the Himalaya-Tibet system: geopoem based on new modelling, geological and geophysical data, *Earth Planet Sc Lett*, *174*(3-4), 397-409.

Cherchi, A., and L. Montadert (1982), Oligo-Miocene rift of Sardinia and the early history of the Western Mediterranean Basin, *Nature*, *298*(5876), 736-739.

Christensen, U. R. (1996), The influence of trench migration on slab penetration into the lower mantle, *Earth Planet Sc Lett*, *140*(1-4), 27-39.

Cloos, M. (1993), Lithospheric buoyancy and collisional orogenesis: Subduction of oceanic plateaus, continental margins, island arcs, spreading ridges, and seamounts, *Geol Soc Am Bull*, *105*(6), 715-737.

Conrad, C. P., and C. Lithgow-Bertelloni (2002), How Mantle Slabs Drive Plate Tectonics, *Science*, *298*(5591), 207-209.

Davies, J. H., and F. Von Blanckenburg (1995), Slab Breakoff - a Model of Lithosphere Detachment and Its Test in the Magmatism and Deformation of Collisional Orogens, *Earth Planet Sc Lett*, *129*(1-4), 85-102.

De Franco, R., R. Govers, and R. Wortel (2008), Dynamics of continental collision: influence of the plate contact, *Geophys J Int*, *174*(3), 1101-1120.

Dewey, J. F., M. L. Helman, S. D. Knott, E. Turco, and D. H. W. Hutton (1989), Kinematics of the western Mediterranean, *Geological Society, London, Special Publications*, *45*(1), 265-283.

Di Giuseppe, E., J. van Hunen, F. Funiciello, C. Faccenna, and D. Giardini (2008), Slab stiffness control of trench motion: Insights from numerical models, *Geochem Geophy Geosy*, *9*.

Di Luzio, E., G. Mele, M. M. Tiberti, G. P. Cavinato, and M. Parotto (2009), Moho deepening and shallow upper crustal delamination beneath the central Apennines, *Earth Planet Sc Lett*, *280*(1-4), 1-12.

Duretz, T., T. V. Gerya, and D. A. May (2011), Numerical modelling of spontaneous slab breakoff and subsequent topographic response, *Tectonophysics*, *502*(1-2), 244-256.

Elsasser, W. M. (1969), Convection and stress propagation in the upper mantle, in *The Application of Modern Physics to the Earth and Planetary Interiors*, S.K. Runcorn, 223-246, Wiley-Inerscience, New York.

Enns, A., T. W. Becker, and H. Schmeling (2005), The dynamics of subduction and trench migration for viscosity stratification, *Geophys J Int*, *160*(2), 761-775.

Faccenna, C., T. W. Becker, F. P. Lucente, L. Jolivet, and F. Rossetti (2001), History of subduction and back-arc extension in the Central Mediterranean, *Geophys J Int*, *145*(3), 809-820.

Faccenna, C., O. Bellier, J. Martinod, C. Piromallo, and V. Regard (2006), Slab detachment beneath eastern Anatolia: A possible cause for the formation of the North Anatolian fault, *Earth Planet Sc Lett*, *242*(1-2), 85-97.

Faccenna, C., A. Heuret, F. Funiciello, S. Lallemand, and T. W. Becker (2007a), Predicting trench and plate motion from the dynamics of a strong slab, *Earth Planet Sc Lett*, *257*(1-2), 29-36.

Faccenna, C., F. Funiciello, L. Civetta, M. D'Antonio, M. Moroni, and C. Piromallo (2007b), Slab disruption, mantle circulation, and the opening of the Tyrrhenian basins, in *Cenozoic Volcanism in the Mediterranean Area*, edited by S. P. Geological Society of America, pp. 153-169.

Faccenna, C., P. Molin, B. Orecchio, V. Olivetti, O. Bellier, F. Funiciello, L. Minelli, C. Piromallo, and A. Billi (2011), Topography of the Calabria subduction zone (southern Italy): Clues for the origin of Mt. Etna, *Tectonics*, *30*(1), TC1003.

Ferrari, L. (2004), Slab detachment control on mafic volcanic pulse and mantle heterogeneity in central Mexico, *Geology*, *32*(1), 77-80.

Forsyth, D., and S. Uyeda (1975), On the Relative Importance of the Driving Forces of Plate Motion, *Geophysical Journal of the Royal Astronomical Society*, *43*(1), 163-200.

Funiciello, F., C. Faccenna, D. Giardini, and K. Regenauer-Lieb (2003a), Dynamics of retreating slabs: 2. Insights from three-dimensional laboratory experiments, *J Geophys Res-Sol Ea*, *108*(B4).

Funiciello, F., G. Morra, K. Regenauer-Lieb, and D. Giardini (2003b), Dynamics of retreating slabs: 1. Insights from two-dimensional numerical experiments, *J Geophys Res-Sol Ea*, *108*(B4).

Funiciello, F., C. Faccenna, A. Heuret, S. Lallemand, E. Di Giuseppe, and T. W. Becker (2008), Trench migration, net rotation and slab-mantle coupling, *Earth Planet Sc Lett*, *271*(1-4), 233-240.

Garfunkel, Z., C. A. Anderson, and G. Schubert (1986), Mantle circulation and the lateral migration of subducted slabs, *J. Geophys. Res.*, *91*(B7), 7205-7223.

Gasperini, D., J. Blichert-Toft, D. Bosch, A. Del Moro, P. Macera, and F. AlbarËde (2002), Upwelling of deep mantle material through a plate window: Evidence from the geochemistry of Italian basaltic volcanics, *J. Geophys. Res.*, *107*(B12), 2367.

Gerya, T. V., D. A. Yuen, and W. V. Maresch (2004), Thermomechanical modelling of slab detachment, *Earth Planet Sc Lett*, *226*(1-2), 101-116.

Giardini, D., and M. Velonà (1991), The Deep Seismicity of the Tyrrhenian Sea, *Terra Nova*, *3*(1), 57-64.

Göğüş, O. H., and R. N. Pysklywec (2008a), Near-surface diagnostics of dripping or delaminating lithosphere, *J. Geophys. Res.*, *113*(B11), B11404.

Göğüş, O. H., and R. N. Pysklywec (2008b), Mantle lithosphere delamination driving plateau uplift and synconvergent extension in eastern Anatolia, *Geology*, *36*(9), 723-726.

Göğüş, O. H., R. N. Pysklywec, F. Corbi, and C. Faccenna (2011), The surface tectonics of mantle lithosphere delamination following ocean lithosphere subduction: Insights from physical-scaled analogue experiments, *Geochem Geophy Geosy*, *12*.

Griffiths, R. W., R. I. Hackney, and R. D. van der Hilst (1995), A laboratory investigation of effects of trench migration on the descent of subducted slabs, *Earth Planet Sc Lett*, *133*, 1-17.

Guillaume, B., F. Funiciello, C. Faccenna, J. Martinod, and V. Olivetti (2010), Spreading pulses of the Tyrrhenian Sea during the narrowing of the Calabrian slab, *Geology*, *38*(9), 819-822.

Guillot, S., E. Garzanti, D. Baratoux, D. Marquer, G. Maheo, and J. de Sigoyer (2003), Reconstructing the total shortening history of the NW Himalaya, *Geochem Geophy Geosy*, *4*.

Gurnis, M., and B. H. Hager (1988), Controls of the Structure of Subducted Slabs, *Nature*, *335*(6188), 317-321.

Hafkenscheid, E., M. J. R. Wortel, and W. Spakman (2006), Subduction history of the Tethyan region derived from seismic tomography and tectonic reconstructions, *J Geophys Res-Sol Ea*, *111*(B8).

Hall, R. (2002), Cenozoic geological and plate tectonic evolution of SE Asia and the SW Pacific: computer-based reconstructions, model and animations, *J Asian Earth Sci*, *20*(4), 353-431.

Hall, R., and W. Spakman (2002), Subducted slabs beneath the eastern Indonesia-Tonga region: insights from tomography, *Earth Planet Sc Lett*, *201*(2), 321-336.

Handy, M. R., and J. P. Brun (2004), Seismicity, structure and strength of the continental lithosphere, *Earth Planet Sc Lett*, *223*(3-4), 427-441.

Hatzfeld, D., and P. Molnar (2010), Comparisons of the Kinematics and Deep Structures of the Zagros and Himalaya and of the Iranian and Tibetan Plateaus and Geodynamic Implications, *Rev Geophys*, *48*.

Heuret, A., F. Funiciello, C. Faccenna, and S. Lallemand (2007), Plate kinematics, slab shape and back-arc stress: A comparison between laboratory models and current subduction zones, *Earth Planet Sc Lett*, *256*(3-4), 473-483.

Houseman, G. A., and L. Gemmer (2007), Intra-orogenic extension driven by gravitational instability: Carpathian-Pannonian orogeny, *Geology*, *35*(12), 1135-1138.

Jacoby, W. R. (1976), Paraffin model experiment of plate tectonics, *Tectonophysics*, *35*, 103-113.

Jin, D., S.-i. Karato, and M. Obata (1998), Mechanisms of shear localization in the continental lithosphere: inference from the deformation microstructures of peridotites from the Ivrea zone, northwestern Italy, *J Struct Geol*, *20*(2-3), 195-209.

Jolivet, L., and C. Faccenna (2000), Mediterranean extension and the Africa-Eurasia collision, *Tectonics*, *19*(6), 1095-1106.

Jolivet, L., R. Augier, C. Faccenna, F. Negro, G. Rimmele, P. Agard, C. Robin, F. Rossetti, and A. Crespo-Blanc (2008), Subduction, convergence and the mode of backarc extension in the Mediterranean region, *B Soc Geol Fr*, *179*(6), 525-550.

Jull, M., and P. B. Kelemen (2001), On the conditions for lower crustal convective instability, *J. Geophys. Res.*, *106*(B4), 6423-6446.

Karato, S., and P. Wu (1993), Rheology of the Upper Mantle - a Synthesis, *Science*, *260*(5109), 771-778.

Kerr, A. C., and J. Tarney (2005), Tectonic evolution of the Caribbean and northwestern South America: The case for accretion of two Late Cretaceous oceanic plateaus, *Geology*, *33*(4), 269-272.

Keskin, M. (2003), Magma generation by slab steepening and breakoff beneath a subduction-accretion complex: An alternative model for collision-related volcanism in Eastern Anatolia, Turkey, *Geophys. Res. Lett.*, *30*(24), 8046.

Knesel, K. M., B. E. Cohen, P. M. Vasconcelos, and D. S. Thiede (2008), Rapid change in drift of the Australian plate records collision with Ontong Java plateau, *Nature*, *454*(7205), 754-U775.

Kohlstedt, D. L., B. Evans, and S. J. Mackwell (1995), Strength of the Lithosphere - Constraints Imposed by Laboratory Experiments, *J Geophys Res-Sol Ea*, *100*(B9), 17587-17602.

Lallemand, S., A. Heuret, and D. Boutelier (2005), On the relationships between slab dip, back-arc stress, upper plate absolute motion, and crustal nature in subduction zones, *Geochem Geophy Geosy*, *6*.

Lambeck, K., and P. Johnston (1998), *The viscosity of the mantle: evidence from analyses of glacial-rebound phenomena*, Cambridge University Press.

Le Pichon, X. (1982), Land-locked ocean basin and continental collision in the eastern Mediterranean area as a case example, in *Mountain building processes*, edited, Academica Press, London.

Lei, J., and D. Zhao (2007), Teleseismic evidence for a break-off subducting slab under Eastern Turkey, *Earth Planet Sc Lett*, *257*, 14-28.

Li, C., R. D. Van der Hilst, A. S. Meltzer, and E. R. Engdahl (2008), Subduction of the Indian lithosphere beneath the Tibetan Plateau and Burma, *Earth Planet Sc Lett*, *274*(1-2), 157-168.

Malinverno, A., and W. B. F. Ryan (1986), Extension in the Tyrrhenian Sea and shortening in the Apennines as result of arc migration driven by sinking of the lithosphere, *Tectonics*, *5*(2), 227-245.

Mann, P., and A. Taira (2004), Global tectonic significance of the Solomon Islands and Ontong Java Plateau convergent zone, *Tectonophysics*, *389*, 137-190.

Martinod, J., F. Funiciello, C. Faccenna, S. Labanieh, and V. Regard (2005), Dynamical effects of subducting ridges: insights from 3-D laboratory models, *Geophys J Int*, *163*(3), 1137-1150.

Matte, P., M. Mattauer, J. M. Olivet, and D. A. Griot (1997), Continental subductions beneath Tibet and the Himalayan orogeny: a review, *Terra Nova*, *9*(5-6), 264-270.

Meissner, R., and W. Mooney (1998), Weakness of the lower continental crust: a condition for delamination, uplift, and escape, *Tectonophysics*, *296*(1-2), 47-60.

Morency, C., and M. P. Doin (2004), Numerical simulations of the mantle lithosphere delamination, *J. Geophys. Res.*, *109*(B3), B03410.

Moresi, L. N., and V. S. Solomatov (1995), Numerical Investigation of 2d Convection with Extremely Large Viscosity Variations, *Phys Fluids*, *7*(9), 2154-2162.

Nicholich, R., and G. V. Dal Piaz (1992), Moho isobaths. Structural Model of Italy. Scale 1:500,000, *Quaderni de "La Ricerca Scientifica"*, *114*(3), CNR, Progetto Finalizzato Geodinamica, Roma.

Petterson, M. G., C. R. Neal, J. J. Mahoney, L. W. Kroenke, A. D. Saunders, T. L. Babbs, R. A. Duncan, D. Tolia, and B. McGrail (1997), *Structure and deformation of north and central malaita, solomon islands: tectonic implications for the Ontong Java plateau-Solomon arc collision, and for the fate of oceanic plateaus*, 33 pp., Elsevier, Amsterdam, PAYS-BAS.

Piromallo, C., and A. Morelli (2003), P wave tomography of the mantle under the Alpine-Mediterranean area, *J Geophys Res-Sol Ea*, *108*(B2).

Piromallo, C., T. W. Becker, F. Funiciello, and C. Faccenna (2006), Three-dimensional instantaneous mantle flow induced by subduction, *Geophys Res Lett*, *33*(8).

Qin, J., S. Lai, and Y. Li (2008), Slab Breakoff Model for the Triassic Post-Collisional Adakitic Granitoids in the Qinling Orogen, Central China: Zircon U-Pb Ages, Geochemistry, and Sr-Nd-Pb Isotopic Constraints, *International Geology Review*, *50*(12), 1080-1104.

Ranalli, G. (1995), *Rheology of the Earth*, 2 ed., Chapman & Hall, London.

Ranalli, G., R. Pellegrini, and S. D'Offizi (2000), Time dependence of negative buoyancy and the subduction of continental lithosphere, *Journal of Geodynamics*, *30*(5), 539-555.

Regard, V., C. Faccenna, J. Martinod, and O. Bellier (2005), Slab pull and indentation tectonics: insights from 3D laboratory experiments, *Phys Earth Planet In*, *149*(1-2), 99-113.

Regard, V., C. Faccenna, O. Bellier, and J. Martinod (2008), Laboratory experiments of slab break-off and slab dip reversal: insight into the Alpine Oligocene reorganization, *Terra Nova*, *20*(4), 267-273.

Regard, V., C. Faccenna, J. Martinod, O. Bellier, and J. C. Thomas (2003), From subduction to collision: Control of deep processes on the evolution of convergent plate boundary, *J Geophys Res-Sol Ea*, *108*(B4).

Replumaz, A., A. M. Negredo, A. Villasenor, and S. Guillot (2010), Indian continental subduction and slab break-off during Tertiary collision, *Terra Nova*, *22*(4), 290-296.

Replumaz, A., H. Karason, R. D. van der Hilst, J. Besse, and P. Tapponnier (2004), 4-D evolution of SE Asia's mantle from geological reconstructions and seismic tomography, *Earth Planet Sc Lett*, *221*(1-4), 103-115.

Ritzwoller, M. H., N. M. Shapiro, and S.-J. Zhong (2004), Cooling history of the Pacific lithosphere, *Earth Planet Sc Lett*, *226*(1-2), 69-84.

Royden, L. H. (1993), The Tectonic Expression Slab Pull at Continental Convergent Boundaries, *Tectonics*, *12*(2), 303-325.

Scarascia, S., R. Cassinis, and F. Federici (1998), Gravity modeling of deep structures in the northern-central Apennines., *Mem. Soc. Geol. It.*, *52*, 231-246.

Schellart, W. P. (2008), Kinematics and flow patterns in deep mantle and upper mantle subduction models: Influence of the mantle depth and slab to mantle viscosity ratio, *Geochem. Geophys. Geosyst.*, *9*(3), Q03014.

Selvaggi, G., and C. Chiarabba (1995), Seismicity and P-wave velocity image of the Southern Tyrrhenian subduction zone, *Geophys J Int*, *121*(3), 818-826.

Séranne (1999), Early Oligocene stratigraphic turnover on the west Africa continental margin: a signature of the Tertiary greenhouse-to-icehouse transition?, *Terra Nova*, *11*(4), 135-140.

Shemenda, A. I. (1993), Subduction of the Lithosphere and Back Arc Dynamics: Insights From Physical Modeling, *J. Geophys. Res.*, *98*(B9), 16167-16185.

Silver, P. G., R. M. Russo, and C. Lithgow-Bertelloni (1998), Coupling of South American and African Plate Motion and Plate Deformation, *Science*, *279*(5347), 60-63.

Speranza, F. (1999), Paleomagnetism and the Corsica-Sardinia rotation: A short review, *Bollettino della Società geologica italiana*, *118*, 537-543.

Stegman, D. R., J. Freeman, W. P. Schellart, L. Moresi, and D. May (2006), Influence of trench width on subduction hinge retreat rates in 3-D models of slab rollback, *Geochem Geophy Geosy*, *7*.

Toussaint, G., E. Burov, and L. Jolivet (2004), Continental plate collision: Unstable vs. stable slab dynamics, *Geology*, *32*(1), 33-36.

Turcotte, D. L., and G. Schubert (2002), *Geodynamics: Applications of continuum physics to geological problems. Second Edition*, Cambridge University Press.

van den Berg, A. P., P. E. van Keken, and D. A. Yuen (1993), The effects of a composite non-Newtonian and Newtonian rheology on mantle convection, *Geophys J Int*, *115*(1), 62-78.

van den Beukel, J., and R. Wortel (1987), Temperatures and shear stresses in the upper part of a subduction zone, *Geophys. Res. Lett.*, *14*(10), 1057-1060.

Van der Voo, R. (1993), *Paleomagnetism of the Atlantic Tethys and Iapetus Oceans*, Cambridge University Press, Cambridge.

van Hunen, J., and M. B. Allen (2011), Continental collision and slab break-off: A comparison of 3-D numerical models with observations, *Earth Planet Sc Lett*, *302*(1-2), 27-37.

van Hunen, J., A. P. van den Berg, and N. J. Vlaar (2000), A thermo-mechanical model of horizontal subduction below an overriding plate, *Earth Planet Sc Lett*, *182*(2), 157-169.

van Hunen, J., A. P. van den Berg, and N. J. Vlaar (2002), On the role of subducting oceanic plateaus in the development of shallow flat subduction, *Tectonophysics*, *352*(3-4), 317-333.

Vermeersen, L. L. A., R. Sabadini, R. Devoti, V. Luceri, P. Rutigliano, C. Sciarretta, and G. Bianco (1998), Mantle viscosity inferences from joint inversions of pleistocene deglaciatio‐induced changes in geopotential with a new SLR analysis and polar wander, *Geophys. Res. Lett.*, *25*(23), 4261-4264.

Vignaroli, G., C. Faccenna, L. Jolivet, C. Piromallo, and F. Rossetti (2008), Subduction polarity reversal at the junction between the Western Alps and the Northern Apennines, Italy, *Tectonophysics*, *450*(1-4), 34-50.

Watts, A. B. (2001), *Isostasy and flexure of the lithosphere*, Cambridge Univerisy Press, Cambridge.

Wong A Ton, S. Y. M., and M. J. R. Wortel (1997), Slab detachment in continental collision zones: An analysis of controlling parameters, *Geophys. Res. Lett.*, *24*(16), 2095-2098.

Wortel, M. J. R., and W. G. Spakman (1992), Structure and dynamics of subducted lithosphere in the Mediterranean region, *Proc. K. Ned. Akad. Wet.,* 95, 325-347.

Wortel, M. J. R., and W. Spakman (2000), Geophysics - Subduction and slab detachment in the Mediterranean-Carpathian region, *Science*, *290*(5498), 1910-1917.

Yoshioka, S., and M. J. R. Wortel (1995), Three-dimensional numerical modeling of detachment of subducted lithosphere, *J. Geophys. Res.*, *100*(B10), 20223-20244.

Zhong, S. J., and M. Gurnis (1995), Mantle Convection with Plates and Mobile, Faulted Plate Margins, *Science*, *267*(5199), 838-843.

Zhong, S. J., M. T. Zuber, L. Moresi, and M. Gurnis (2000), Role of temperature-dependent viscosity and surface plates in spherical shell models of mantle convection, *J Geophys Res-Sol Ea*, *105*(B5), 11063-11082.

ACKNOWLEDGMENTS

First of all, I would like to thank the three people that made this thesis possible: Claudio, Francesca and Jeroen. Thanks to all of you, it's hard to find better people to work with. Your enthusiasm and passion for science has been source of inspiration for me. Thanks for providing the best environment for me to grow up both from the professional and personal point of view. I am truly glad to work with you.

Claudio, thanks for sharing with me your wide knowledge of geology and your ideas, talk to you is always inspiring. Also, thanks for the many times you enter the PhD student room saying "Bella la vita, eh!", that always made me smile.

Francesca, you always know what to do, each time I had a problem, a question or a simple doubt I knew I could ask you. I really thank you for that and for always being so nice and supportive during these three years.

Jeroen, thanks for your dedication and patience in teaching me so many things. Your help has been essential for me and for this thesis. Also, thanks for being always available for discussions and suggestions, even though we were in different countries, I really appreciated it.

Most of the thesis has been possible thanks to the computational resources provided by the HPC grants of CASPUR and Durham University.

A big thanks to my family: my mom, my dad and my brother, who keep supporting me and my choices, no matter how weird the subject of my research is.

A special thanks to the wonderful friends that I found in Durham: Alex, Claudia, Michele, Sabina and Iona.

I would like to thank Erika for being the best partner at every conference.

A huge hug to Carlotta, Rolfi, Alice and Pach. You guys are my solid rock, even though you think it is the other way around.

Many thanks to my "bolognesi" friends: Fede, Vero, Eli, Engri, Jacopo and Andrea. We live in different parts of the world, but somehow it is like we never left Bologna and I love that.

And, finally, to my amazing roman family: Betta, Stella, Isa, Monia, Mannino, Fabietto, Magico, Andrea and Peppe. You made Rome my home. To you guys I dedicate my thesis.